**Ph.D. degree in Systems Medicine**

**Curriculum in Human Genetics**

**European School of Molecular Medicine (SEMM),**

**University of Milan and University of Naples "Federico II"**

**Settore MED/03**

# Gene therapy for gyrate atrophy of choroid and retina and for USH1B retinitis pigmentosa

*Fabio Dell'Aquila*

TIGEM, Naples

Matricola R12094

***Tutor***: Prof. Alberto Auricchio

Dept. of Advanced Biomedicine, Federico II University;

TIGEM, Naples, Italy

***Internal Supervisor***: Prof. Ivan Conte

Dept. Of Biology, Federico II University;

TIGEM, Naples, Italy

***External Supervisor***: Prof. Valeria Marigo

Dept. of Life Sciences, Università degli Studi di Modena e Reggio Emilia;

Modena, Italy

Anno accademico 2021-2022

## ACKNOWLEDGEMENTS

"**To Alberto and Rita,**

How you live the journey is more important than meeting your goals. Ours has not been easy in the beginning but I am proud of what we accomplished and of what scientist I've become by following and stealing your teaching. Thank you from the bottom of my heart.

**To my family at home,**

When they abandon, we rejoice; in sickness, we heal; when we feel lost, we love. Thank you for teaching me the essentials of life and to help me pursue my dream.

**To Renato, Manel y Alessio,**

Brothers may part, but they will always sustain and cheer each other, praise for successes, aid for failures. I could not ask for anything rarer than our friendship.

**To Federica and my family in the lab,**

Whenever I felt abandoned and lost, you were always there in loving support. You played the most important part in this journey, although I was not giving you ¼ of what you deserved. We will always share something precious that no other group will ever experience.

**To Eva D. Mar.,**

You taught me friends are here today, in a week or in a year, and forever. They will not search for excuses to avoid you and will spare 2 minutes just to check on you. Thank you for allowing me to appreciate the real things in life. I will always be ready to set sail and cook while you seek treasures!

**To Lele Castello**,

You were always in the front line for us, teaching and protecting us instead of caring more about yourself when it was needed. You were always more than a tutor, more than a scientist. Now you are starting a new journey and I cannot be helped to feel a bit sad that I will not see how incredibly good you will perform. 'Till we meet again!

**To S.P.,**

Thank you for shedding light when darkness prevailed."

*Toast to the ones here today,*

*Toast to the ones that we lost on the way.*

# INDEX

## LIST OF ABBREVIATIONS

IRDs: inherited retinal degenerations

AAV: adeno-associated viral

GA: gyrate atrophy of the choroid and retina

USH1B: Usher syndrome type 1B

*OAT*: *ornithine aminotransferase*

CMV: cytomegalovirus

CDS: coding sequence

RPE: retinal pigment epithelium

h*OAT*: *human ornithine aminotransferase*

AAV8: AAV serotype 8

h*MYO7A*: human *myosin 7A*

Sh1: shaker1

PRs: photoreceptors

RP: retinitis pigmentosa

PLP: pyridoxal 5'-phosphate

USH: Usher syndrome

USH1: Usher syndrome type 1

USH2: Usher syndrome type 2

USH3: Usher syndrome type 3

GT: gene therapy

ERG: electroretinogram

SD-OCT: spectral domain optical coherence tomography

IV: intravenous

RGCs: retinal ganglion cells

SR: sub-retinal

SC: suprachoroidal

ITRs: inverted terminal repeats

ORFs: open reading frames

AAP: assembly activating protein

ONL: outer nuclear layer

INL: inner nuclear layer

LCA2: Leber congenital amaurosis type 2

RPE65: isomerase RPE-specific 65 KDa protein

SD: splicing donor

SA: splicing acceptor

WB: western blot

WPRE: Woodchuck hepatitis virus post-transcriptional regulatory element

BGH: bovine growth hormone

CAG: modified version of the CMV early enhancer/chicken β actin promoter

CBA: chicken beta-actin

SV40: simian virus 40

P188: poloxamer 188

GC: genome copies

EGFP: enhanced green fluorescent protein

GMP: good manufacturing practices

PBS: phosphate buffer saline

DMEM: Dulbeccos' modified Eagle medium

FBS: fetal bovine serum

PMSF: phenylmetanesulfonyl fluoride

RT: room temperature

ANOVA: one-way analysis of variance

p*OAT*: plasmid encoding for human *ornithine aminotransferase*

p*OAT*-3XFlag: plasmid encoding for human *ornithine aminotransferase* 3XFlag tagged

pEGFP: plasmid encoding for enhanced green fluorescent protein

P5C: pyrroline 5-carboxilate

GLU: glutamate

α-KG: α-ketoglutarate

PMP: pyridoxamine-phosphate

CI: chimeric intron

SEM: standard error of mean

SB: southern blot

BP: base pair

GLP: good laboratory practices

HD: high dose

MD: medium dose

LD: low dose

NHPs: non-human primates

## FIGURES AND TABLE INDEX

## ABSTRACT

Inherited Retinal Diseases (IRDs) represent a major cause of blindness worldwide. Adeno-associated viral (AAV) vector-based gene therapies represent the most promising treatments. Here, we aimed to develop AAV vector-based gene therapies for two rare IRDs: gyrate atrophy of the choroid and retina (GA) and Usher syndrome type 1B (USH1B).

GA is characterized by *ornithine aminotransferase* [*OAT*, coding sequence (CDS) ∽1.3 Kb] deficiency. OAT loss-of-function induces a specific toxic effect in retinal pigment epithelium (RPE) cells. In preliminary plasmid transfection experiments, we demonstrated *in vitro* expression and activity of 3XFlag-tagged human *OAT* (h*OAT*-3XFlag) under the control of a CMV promoter (CMV-h*OAT*-3XFlag). We then subretinally injected C57BL/6 mice with an AAV serotype 8 vector containing the CMV-h*OAT*-3XFlag (AAV8-CMV-h*OAT*-3XFlag) construct and confirmed successful *in vivo* expression. Moreover, sub-retinal injection improved retinal outer nuclear layer thickness in $Oat^{tm1DVa}$ ($Oat^{-/-}$) mice, a GA model.

Bi-allelic mutations in the *Myosin7A* gene (*MYO7A*) (CDS ∽6.7 Kb) give rise to USH1B, the most common combination of inherited congenital deafness and early blindness. The *MYO7A* expression cassette exceeds AAV DNA cargo capacity. To overcome this, we split the human *MYO7A* (h*MYO7A*) expression cassette across a dual AAV vector system, which exploits DNA inter-molecular recombination to reconstitute the full-length protein expression. Upon sub-retinal injection of dual AAV8-CBA-h*MYO7A*, we efficiently rescued structural abnormalities in the shaker-1 mouse (sh1), a model of USH1B. During the AAV production process, we found a contaminant vector resulting from recombination between two similar sequences in the AAV8 vector encoding the 5' half of h*MYO7A* (AAV8-5'h*MYO7A)*. This was removed by changing one of the two sequences while maintaining the same MYO7A expression levels *in vivo*. We used sh1 mice to conduct a dose-response analysis and confirm the biological potency and stability of the dual AAV8-h*MYO7A* lot that we will use to treat USH1B subjects. Three selected doses induce expression of full length h*MYO7A*, show dose-dependent effects in improving sh1 abnormalities, and will provide a basis for clinical translation to treat patients with USH1B.

Overall, these studies offer promising results, paving the way for a gene therapy of GA and for the clinical translation of dual AAV vectors in USH1B subjects.

# INTRODUCTION

## 1. The retina and inherited retinal degenerations

The retina is the tissue within the eye deputed to capture and convert light in an electrical signal that is interpreted by the central nervous system to form images. The biochemical processes that convert light into electrical signals are initiated by two different cell types:

- rods and cones photoreceptors (PRs), which are specialized post-mitotic cells that convert light in an electrical signal [1]
    - rods have higher light sensitivity and are required for night and peripheral vision
    - cones are important for color vision and vision acuity
- retinal pigment epithelial (RPE) cells, which support PRs by supplying them with nutrients, recycle of biomolecules from the visual pathways and create a barrier between the bloodstream (choroid) and the neuroretina, which is comprised of PRs and other neuronal cells that generate the electrical signal and send it to the visual cortex [2] (Fig. 1). Additionally, RPE cells allow to capture light and protect the retina from photo-oxidative stresses due to the black pigment stored inside melanosomes vesicles [3].

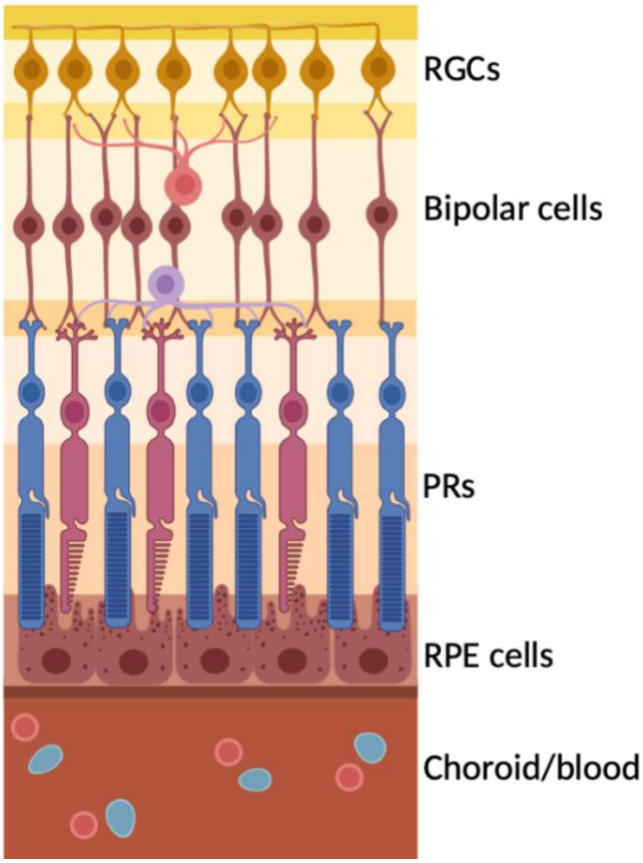


***Figure 1: Simple anatomy of the retina***

The cartoon shows the main retinal cell types and their interconnections. RGCs: retinal ganglion cells; PRs: photoreceptors; RPE: retinal pigment ephitelial cells. Image done using biorender.com

In recent years, blindness has entered the top three worst pathological conditions (Fig. 2), possibly due to technological advancements that require sight such as smartphones and computers [4].

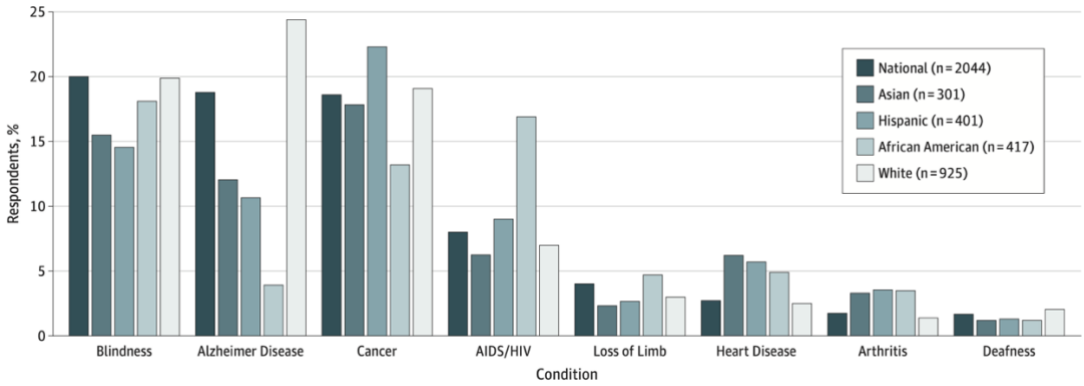


***Figure 2: Ranking of worst pathological conditions***

*Survey was conducted in the US and results were divided by ethnicity. Results are shown as % of respondents. Image from (Scott et al., 2016)* [4].

Inherited diseases that progressively lead to reduced vision and blindness are referred to as inherited retinal degenerations (IRDs). This group of diseases is becoming an increasingly important social and economic issue, with a prevalence of up to 1 individual into 2000 individuals and over 2 milion affected people [5]. IRDs are mostly monogenic and, to date, 330 genes have been associated with IRDs (https://sph.uth.edu/retnet/home.htm) and this number is increasing yearly thanks to technologies like whole genome sequencing. Many mutations causing IRDs affect RPE, PRs or both. Diseases affecting the RPE decrease PR function, like gyrate atrophy of the choroid and retina, slowly leading to retinal degeneration and blindness. In other diseases, like Usher syndrome type 1B, retinal degeneration hits PRs as well.

### 1.1 Gyrate atrophy of the choroid and retina

Gyrate atrophy of the choroid and retina (gyrate atrophy or simply GA, MIM#258870) is a rare inherited chorioretinal disease and a blinding disorder, first described as an atypical retinitis pigmentosa (RP) [6]. Patients affected by GA first experience loss of night vision and visual acuity, like in RP [7]. Ocular fundoscopy in patients revealed that degeneration starts in RPE cells from the periphery of the retina; patients experience patchy vision corresponding to the areas where RPE cells are still present [8] [9]. As the disease progresses, these lesions increase in size and number and move towards the center of the retina. Cataract is also a common feature of the disease [9]. During the fifth-sixth decade of life, GA subjects lose vision completely [7]. A recent study calculated the theoretical worldwide prevalence of GA, estimating a prevalence of 1 affected individual:1500000 [10];

interestingly, GA is much more frequent in Finland (1 individual:50000), possibly due to a founder mutation effect, and indeed one third of all GA cases are Finnish [7].

The causative gene of GA, *ornithine aminotransferase* (*OAT*, MIM#613349), encodes a reversible mitochondrial enzyme involved in ornithine conversion or synthesis. Ornithine aminotransferase (OAT) monomers form an active homodimer that requires piridoxal 5'-phosphate (PLP), a derivative of vitamin B6, as a cofactor; active homodimers are able to reassemble into a mature homoexameric state [11]. This enzyme is widely expressed in many tissues across species and in the eye it is expressed both in the RPE and in PRs [12]–[14]. Lack of OAT in the adult life causes hyperornithinemia (Fig. 3) and a specific toxic effect in RPE cells. Only a few patients develop sub-clinical effects in skeletal muscle and the central nervous system [15]–[18]. Interestingly, the worst cases of GA manifest defects of the urea cycle during the neonatal stage of life instead of increases in ornithine levels; infants experience vomiting, encephalopathy and paradoxical low levels of ornithinemia [19]. Further studies on a mouse model of GA lacking Oat expression confirm that the enzyme reaction is shifted towards ornithine synthesis in the first stages of life to generate a source of arginine, required to form urea and correctly expel ammonia (Fig. 3); without OAT activity, homozygous pups die of hyperammonemia a few days after birth unless they receive intra-peritoneal injections of arginine until adulthood [20].

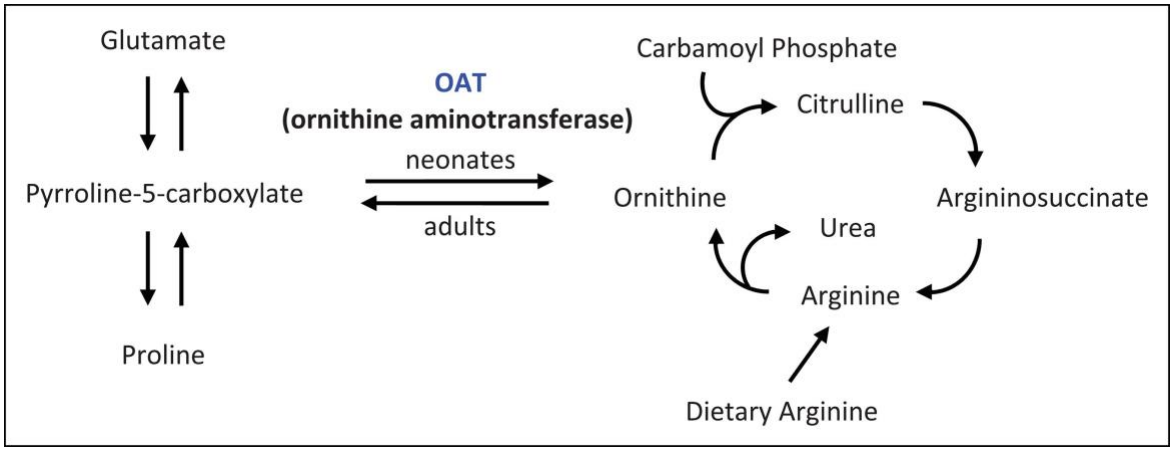


***Figure 3: Schematic representation of OAT activity in different stages of life***

OAT catalyzes the production of ornithine to supply the urea cycle with arginine in the neonatal stage of life and correctly expel ammonia through urea; in the adult life, arginine is supplied by food intake and endosynthesis and OAT reaction shifts towards ornithine conversion to pyrroline-5-carboxilate for aminoacid biosynthesis. Figure from (Palanza *et al.*, 2016) [21].

Clinical trials explored the use of an arginine-restricted diet after the neonatal stage of life to normalize ornithinemia levels. However, in those patients that were able to follow such a strict diet, the treatment only temporarily slowed down disease progression [22].

### 1.2 Usher syndrome type 1B

Usher syndrome (USH) is a rare inherited disorder causing sensorineural hearing loss, RP, and, in some cases, vestibular dysfunction. Although it is relatively rare in humans, it is the most frequent cause of deaf-blindness, accounting for more than 50% of individuals who are both deaf and blind [23], [24], about 18% of RP cases [25], and 5% of all cases of congenital deafness [26]. USH is classified in three categories: Usher syndrome type 1 (USH1), the most severe form, consisting of profound hearing loss and vestibular dysfunction from birth and earlier onset of RP than other forms of USH; Usher syndrome type 2 (USH2), which produces less severe congenital hearing loss and does not impair normal vestibular function; Usher syndrome type 3 (USH3), a less common form, is characterized by progressive and variable vestibular dysfunction and onset of RP [27]. USH1 accounts for approximately one-third of USH patients. Among these, Usher Syndrome type 1B (USH1B, MIM#276900) accounts for up to 50% of all USH1 cases, with a prevalence of 1:30000 to 1:42000. [23], [24], [28]. USH1B subjects are born with hearing impairment or completely deaf [29]. Retinal defects are clinically measurable at 2-3 years of age. Rod PRs (required for night vision and peripheral vision) are the primary injured cells and start to degenerate earlier than cone PRs (required for color vision and vision acuity), leading to night blindness. As degeneration proceeds, patients will lose cones as well and will progressively lose peripheral vision, ultimately ending up in blindness [29]. Although hearing loss can be counteracted by cochlear implant surgery, no treatment is available for RP.

USH1B is caused by biallelic mutations in the *Myosin 7A* (*MYO7A*, MIM#276903) gene [29], which encodes for a cargo motor protein. Myosin7A (MYO7A) protein in the retina is localized in (i) the RPE to transport melanosomes to the apical villi (ii) the connecting cilium of rod PRs to recycle rhodopsin back to the outer segment [30]–[32]. Although USH1B is classified as a rod-cone dystrophy, the pathogenesis of the disease is yet to be clarified, as the only available animal models of USH1B (rodents) do not show frank retinal degeneration; interestingly, MYO7A co-localizes with calyceal processes only in primates rods' connecting cilium, thus it is possible that mouse models do not show retinal degeneration due to structural differences [33].

## 2. Gene therapy

Gene therapy (GT) is able to treat patients of inherited disorders by delivering genetic material into cells using a suitable vector. GT strategies typically express a missing gene or induce silencing of a toxic product. An ideal gene therapy vector should have the following features: i) the ability to localize to target cells and release their genetic material inside the nucleus; ii) provide long-term expression of the transgene; iii) have sufficient DNA capacity to package the required genetic material; iv) elicit low to no toxicity. Given these conditions, several non-viral and viral vectors have been investigated to treat IRDs. Viral vectors like adeno and lentiviral vectors are able to induce transgene expression in RPE cells but poorly transduce PRs [34]. Non-viral vectors are able to target both cell types but show low transgene expression and/or transient gene-expression compared to viral vectors [35] [36].

After years of pre-clinical studies, adeno-associated viral (AAV) vectors have been selected as the perfect candidate for ocular gene transfer. AAVs are small, non-integrating particles able to diffuse and bind retinal target cells. Although AAV vectors genomes stay episomal and do not integrate, they induce long-lasting transgene expression after a single administration [37], [38]. Additionally, retinal cells are predominantly post-mitotic, favoring the use of a non-integrative vector.

### 2.1 Gene therapy of inherited retinal diseases

The eye has several positive characteristics for the application of gene therapy, particularly with viral vectors. The eye is a compact, enclosed organ [39], therefore gene therapy vectors injected in the eye stay highly concentrated, enhancing cellular transduction. The tight junctions at the border between the choroid and the RPE impede cells entrance into the internal compartment of the eye, like lymphocytes and white blood cells [40], [41]. Thanks to the unique characteristics of the eye and its transparency, many *in vivo* clinical techniques have been developed to measure retinal activity and ensure correct retinal morphology. These techniques include the electroretinogram (ERG), which measures the electrical activity of PRs and other cell types of the retina; spectral-domain optical coherence tomography (SD-OCT), which uses the same principle of an axial tomography to take scans of the different layers of the retina; and fundoscopy to image the fundus of the eye and check gross alterations of the retina. All these techniques are available in the clinics and were developed for animal models of IRDs as well. These allow to test lead candidate

treatments to be tested in small mouse models before doses are translated to humans; doses are scaled according to the extrapolation that the human retinal surface is around 100-fold larger than that of mice [42], [43]. Therefore, doses used in human eyes are typically 100-fold higher than those used in mice.

The two main routes to administer gene therapy products to retinal cells are intravitreal and subretinal injections (Fig. 4). The intravitreal (IV) injection is considered less invasive, although the medicinal product will likely only come into contact with the most exposed cells due to anatomical barriers, which are retinal ganglion cells (RGCs); moreover, if part of the product remains in the vitreous it is possible to elicit an inflammatory response [44], [45]. The second route of administration is the subretinal (SR) injection, performed under the RPE, which results in partial detachment of the retina in order to reach PRs; the detachment typically resolves in hours or days upon absorption of the injected bleb in patients [45]. A new injection route is represented by the suprachoroidal (SC) injection, where the medicinal product is injected between the choroid and the RPE to reach PRs without causing retinal detachment [46], [47] (Fig. 4). Up to date, more studies are required to explore the use of SC injection in humans for gene therapy approaches.

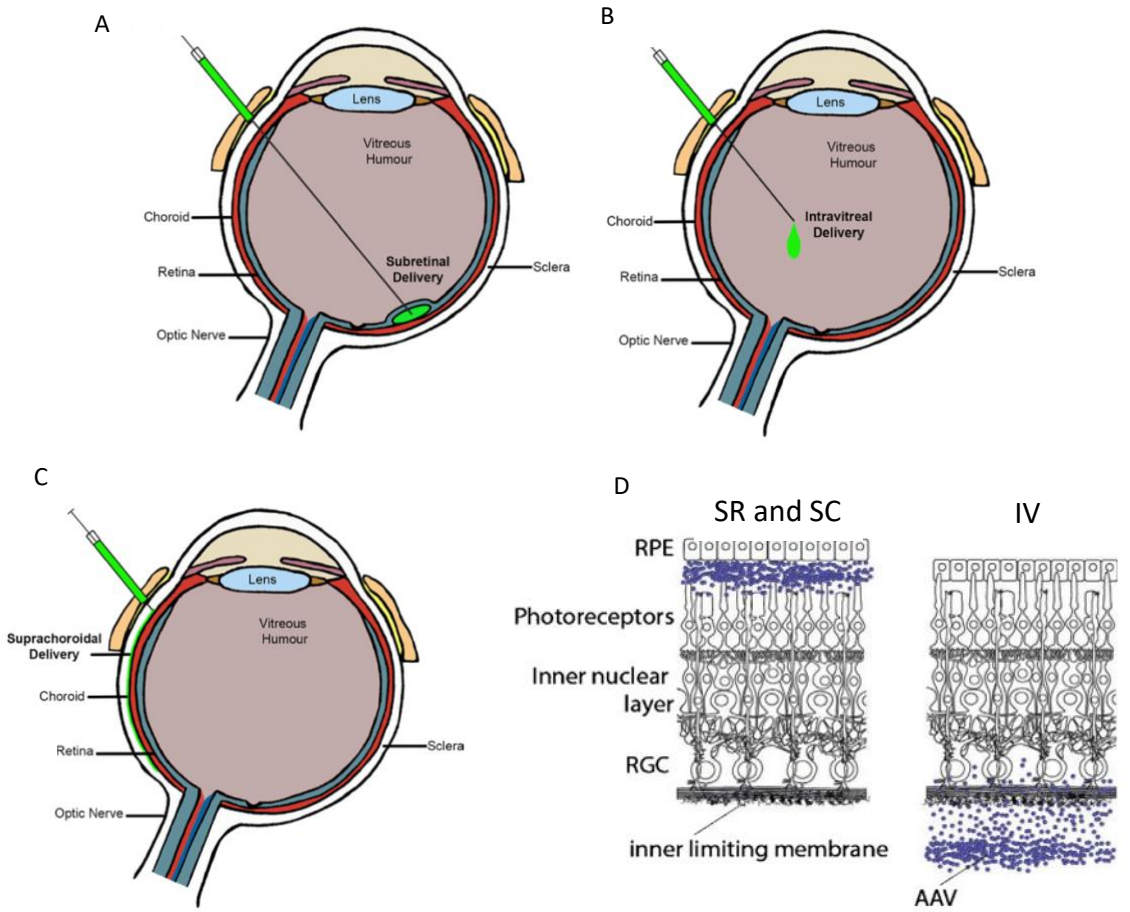


***Figure 4: Explanatory material of trans-scleral subretinal, intravitreal or suprachoroidal injection of AAV particles***

Representative pictures of **(A)** subretinal injection, **(B)** intravitreal injection or **(C)** suprachoroidal injection (image from Guimaraes *et al.*, 2021) [48]. **(D)** AAV particles can transduce RPE and PRs upon subretinal or suprachoroidal injection, while the intravitreal injection targets mainly retinal ganglion cells (RGCs) (image modified from Dalkara&Sahel, 2014) [49]. SR: subretina; SC: suprachoroidal; IV: intravitreal.

## 3. Adeno-associated viral vectors

### 3.1 AAV biology

AAV is a small (20-25 nm in diameter), non-enveloped, icosahedral virus that packages a single strand DNA of 4.7 Kb [50]. It belongs to the Parvoviridae family and is sub-classified as a dependovirus, because it can replicate in target cells only upon co-infection of a helper virus. Indeed, it was originally isolated as a contaminant of adenoviral cultures and thus given the name adeno-associated virus. The AAV genome is flanked by two palindromic inverted terminal repeats (ITRs) that are 145 nucleotides in length and includes two non-overlapping open reading frames (ORFs) encoding for 2 genes, Rep and Cap [37] (Fig. 5). Rep encodes proteins involved in the replication of the viral DNA and packaging of newly synthesized single stranded AAV genomes; Rep induces AAV genome integration in the

AAVS1 locus on human chromosome 19. The Cap gene encodes for VP1, VP2 and VP3 proteins that form the viral capsid. A newly discovered protein named assembly activating protein (AAP) encoded by an alternative ORF within the Cap gene has also been described; AAP targets newly synthesized capsid proteins to the host cell nucleus, aiding the formation of new virions [51].

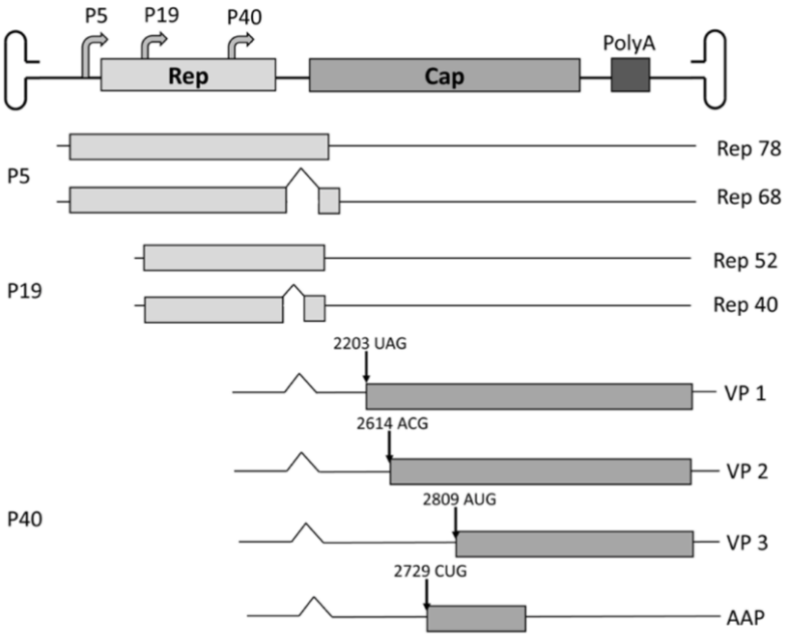


***Figure 5: Wild type genome of adeno-associated viruses***

A single stranded 4.7 kb DNA molecule is packed inside the AAV capsid. Two inverted terminal repeats of 145 bp flank the genome that consists of two open reading frames (ORFs). From left to right: the first ORF encodes for Rep 68, Rep 78, Rep 52 and Rep 40, which coordinate viral replication; the second ORF encodes capsid proteins VP1-2-3 or alternatively the assembly activating protein AAP.

AAV-mediated transduction takes place after a cascade of steps in the cell. First, AAVs bind different receptors and co-receptors on the cell surface, depending on the capsid serotype [52]. Then, AAVs enter the cell through endocytosis. To reach the nucleus, viral particles need to escape both from the endocytic compartment and proteasomal degradation [53], [54]. The capsid uncoats to release the single strand DNA inside the nucleus [55] and start second-strand synthesis, ultimately resulting in transcription and expression of the viral genome [56]. AAV genomes may undergo integration mediated by Rep proteins into the human chromosome 19, in the Rian locus [57]. In the case of recombinant AAVs, which lack the rep gene, there is a very low chance of viral genome integration and tend to stay episomal inside the nucleus [58].

The first recombinant AAV vector was generated by Samulski *et al.* in 1982 [59]. Only the two ITRs are necessary for the encapsidation of the genome while other sequences can be provided in trans for virus production (Fig. 6). This characteristic allows the substitution of 95% of the original genome (except for the ITRs) with a DNA sequence of interest. Despite this fact that nearly all the genome can be substituted, the limited DNA cargo capacity of AAVs remains a significant drawback, restricting expression cassettes to < 5 Kb.

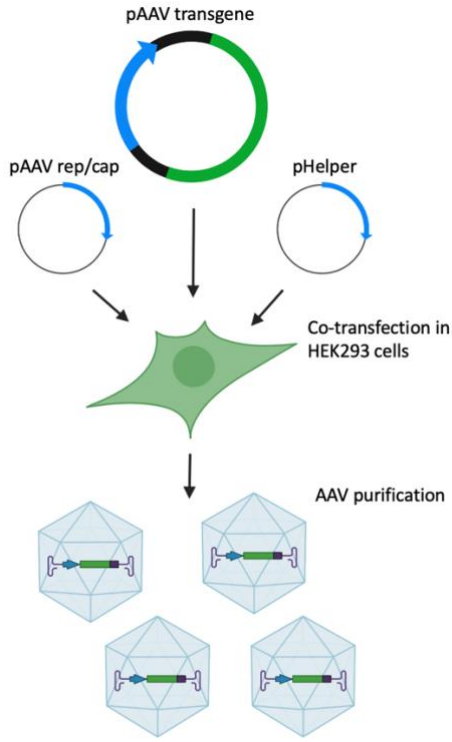


***Figure 6: Adeno-associated viral vector production by triple transfection of HEK293 cells*** HEK293 expressing adenoviral genes E1a and E1b are co-transfected with plasmids encoding for: the remaining adenovirus helper genes E2A and E4 (pHelper); the AAV *rep*/*cap* sequences (pAAVrep/cap); the transgene expression cassette between the AAV2 ITRs (pAAV transgene). Image done using biorender.com

### 3.2 Natural and recombinant AAV serotypes to infect the retina

Hundreds of natural and engineered AAV capsids have been identified [60] [61], each with different transduction properties in terms of cell tropism, immunological reactions and expression levels of the transgene. AAV2 is the most well-known AAV, as many species develop natural infection with this serotype generating antibodies against the viral capsid [62]. Nevertheless, mammals are natural hosts of wild type AAVs and they are not associated with any disease in humans, leading to the exploitation of AAVs for their ability to transduce both dividing and non-dividing cells [63]. To date, the most used AAV vectors are hybrids carrying serotype 2 ITRs and capsid from different variants (AAV 2/n, where the

first number refers to the ITRs and the second to the capsid). The final vector has the safety and versatility advantages of AAV2 while achieving specific cell tropisms that depend on the capsid [64]. Several independent groups have focused on researching and developing AAV capsids that efficiently transduce retinal cells. Upon subretinal delivery, many AAV hybrids are able to efficiently transduce RPE cells, possibly due to the phagocytic nature of this retinal layer or to the expression of particular co-receptors [38]. However, the majority of IRDs specifically affect PRs (either alone or in combination with other cell types) [38]. AAV2/5, 2/7 and 2/9 are able to transduce both RPE and PRs [65], [66] but the most efficient hybrid for this task is AAV2/8, which shows high levels of transgene expression across murine [65], porcine [67], canine [68] and non-human primate retina [69] (Fig. 7).

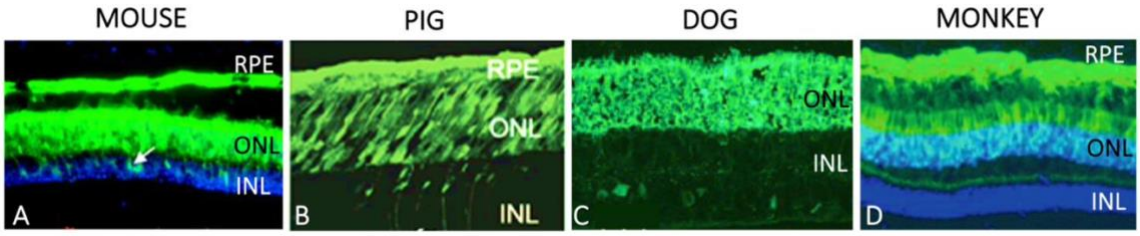


***Figure 7: Transduction of murine, porcine, canine and non-human primate retina driven by AAV2/8***

Fluorescence pictures of C57BL/6 mouse (**A**), pig (**B**), dog (**C**), and non-human primate retinas transduced by AAV2/8 carrying the expression cassette for the enhanced green fluorescent protein. RPE: retinal pigment epithelium, ONL: outer nuclear layer; INL: inner nuclear layer. White arrows: Müller cell nuclei. [Modified from (Allocca *et al.*, 2007) (A) [65], (Mussolino *et al.*, 2011) (B) [67], (Stieger *et al.*, 2008) (C) [68], (Vandenberghe *et al.*, 2011) (D) [69]].

### 3.3 Gene therapy clinical trials of IRDs with AAV vectors

In recent years, the potential of AAV vectors to treat IRDs came to light following the successful treatment of Leber Congenital Amaurosis type 2 (LCA2), a disorder leading to blindness during childhood [70], [71]. RPE cells of LCA2 patients degenerate due to lack of the isomerase RPE-specific 65 KDa protein (RPE65). Pre-clinical studies showed disease rescue in a canine model of LCA2 using an AAV2 carrying the expression cassette for RPE65. These results led 3 independent groups to start gene therapy clinical trials for LCA2 [72]–[74]. Despite result variability across the 3 studies (due to differences in expression cassette sequences, AAV manufacturing and purification, clinical protocols and patients' selection), they all showed positive results. In the best performing of these clinical trials investigators performed re-injection in the contralateral, previously uninjected eye. Notably, the second

administration was well tolerated and patients gained prolonged functional improvement for up to 3 years [75], demonstrating for the first time that AAVs could be readministered to the human subretinal space in the absence of clinically relevant immune responses [76]. After these encouraging results, a Phase III trial was initiated which showed significant improvements with respect to a newly set-up clinical endpoint: the multi-luminance mobility test, in which patients navigate in a randomized environment under variable luminance conditions. Based on these data, in December 2017 the American Food and Drug Association approved the commercialization of voretigene neparvovec (Luxturna), the first gene therapy product for an inherited disease in the USA [77] followed by the European Medicinal Agency in 2018. Following this success, the use of AAVs has been expanded to a number of trials to treat inherited and acquired blinding conditions, further confirming the safety and efficacy of AAV in the retina [78]. A gene therapy for choroideremia with AAV2, namely timrepigene emparvovec, has also shown significant improvement with no adverse event and is currently in phase III clinical development [79]. Recently, a clinical trial of gene therapy for Leber hereditary optic neuropathy showed bilateral visual improvement after unilateral eye administration [80]. Other trials with AAV are targeting wet age-related macular degeneration [81], X-linked retinoschisis [82] and X-linked retinitis pigmentosa (clinical trial ref. #NCT03252847).

## 4 Strategies to expand AAV DNA cargo capacity

Based on the above described successes, AAVs are considered the preferred gene therapy vectors for IRDs. However, many IRDs arise due to mutations in genes with CDS > 5Kb, exceeding the AAV DNA cargo capacity, like USH1B (*MYO7A* CDS ⌣6,7 Kb). Nevertheless, the inherent tendency of AAV genomes to undergo intermolecular concatemerization [58] may be exploited to transfer large genes *in vivo* by splitting the expression cassette into halves, <5 kb in size, each packed in one of two independent AAV vectors (dual AAV) [83]–[86]. In the dual AAV trans-splicing strategy, the expression cassette is divided into two halves and a splice donor (SD) signal is placed at the 3’ end of the 5’-half vector and a splice acceptor (SA) signal at the 5’ end of the 3’-half vector (Fig. 8). Upon co-infection of the same cells and ITR-mediated tail-to-head concatemerization of the halves, the subsequent splicing results in the production of a mature mRNA that encodes a full-size protein [85]. Trans-splicing has been successfully used to express large genes in muscle and retina [87], [88]. However, the transduction efficiency of this system has been found to be lower than

that of a single intact AAV vector, as it is impacted by a number of factors: (i) gene splitting site, as the surrounding sequences can influence the splicing efficiency; (ii) levels of co-infection reached in the cells; (iii) formation of the concatemers in the tail-to-head orientation and (iv) transcription and splicing across the complex structure formed by the ITRs upon concatemerization. Alternatively, dual AAV vectors may contain homologous overlapping sequences (at the 3’ end of the 5’-half vector and at the 5’ end of the 3’-half vector, termed dual AAV overlapping), which, in a cell co-infected by both vectors, could mediate the reconstitution of a large expression cassette by homologous recombination [83] (Fig. 8). The success of this strategy, however, largely depends on the recombinogenic properties of the transgene overlapping sequences. Thus, only genes that contain a highly recombinogenic region are able to achieve therapeutic levels of expression [89]. To overcome this problem, a third dual AAV strategy, namely hybrid, was developed. This strategy is based on the addition of a highly recombinogenic sequence to the trans-splicing vector to increase recombination between the dual AAVs (Fig. 8). In our lab, we have used the highly recombinogenic sequence derived from the lambda phage F1, namely AK [86]. This exogenous sequence is placed downstream of a SD signal in the 5'- half vector and upstream of a SA signal in the 3'-half vector (Fig. 8) to generate the mature transcript while splicing out any unwanted sequence. Additionally, the efficiency of this strategy is transgene-independent as reconstitution of the full-length cassette relies on the recombination mediated by the exogenous homology region.

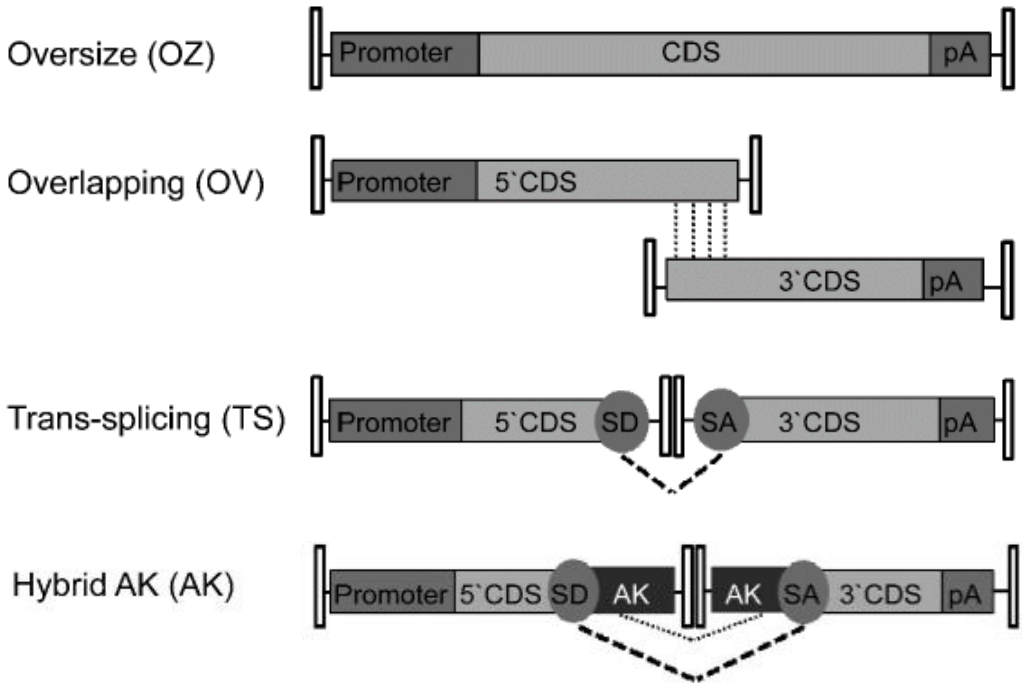


***Figure 8: Schematic representation of AAV-based strategies for large gene transduction***

CDS: coding sequence; pA: poly-adenylation signal; SD: splicing donor signal; SA: splicing acceptor signal; AK: F1 phage recombinogenic. Image from (Trapani *et al.*, 2014) [86].

Notably, dual AAV vectors approaches are particularly suitable for the use in the eye as the small and enclosed environment favors co-infection of 2 independent vectors. In our lab, we were able to confirm efficient reconstitution of CDS > 5 Kb in the eye of small and large animal models upon sub-retinal delivery of dual AAV 2/8 vectors [86], [90], [91]. Importantly, we found that dual AAV2/8 hybrid vectors encoding for human *MYO7A* (h*MYO7A*, from now on referred to as dual AAV-h*MYO7A*) efficiently reconstitute hMYO7A in the mouse RPE and PRs to levels resulting in significant improvement to retinal defects in the shaker1 (sh1) mouse model of USH1B [86], [90]. This mouse model is characterized by an early stop codon in murine *Myo7a* preventing protein expression, which results in mis-localized melanosomes that do not enter RPE apical villi as well as rhodopsin accumulation in rods' connecting cilium [30]–[32]. Due to structural differences between human and murine rods PRs, sh1$^{-/-}$ do not show retinal degeneration [33]. Our group demonstrated reconstitution of human *MYO7A* upon sub-retinal injection of dual AAV-h*MYO7A* (Fig. 9A) which improves the number of correctly localized RPE melanosomes (Fig. 9B-C) and reduces rhodopsin accumulation at the connecting cilium (Fig. 9D).

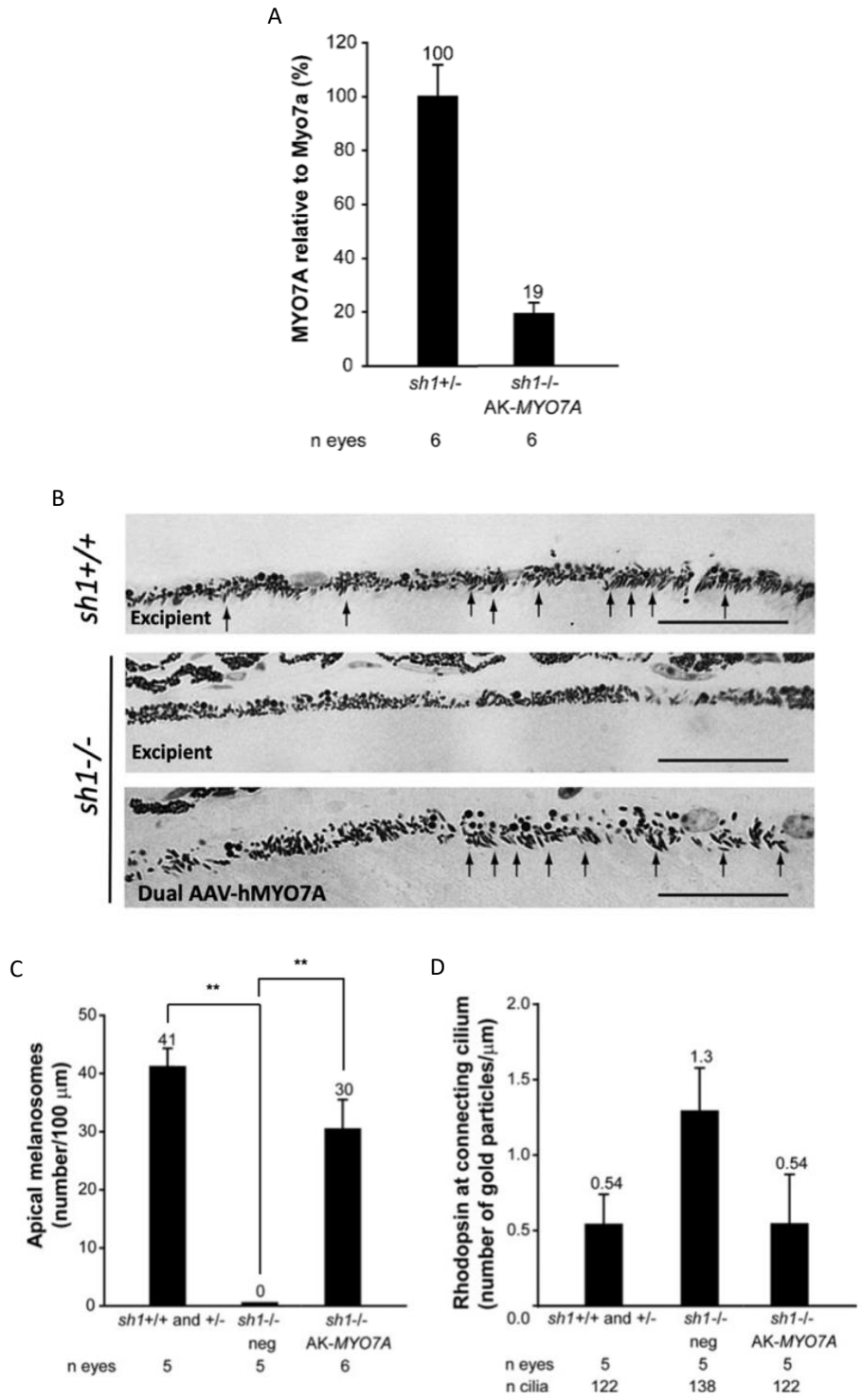


**For figure 9 caption see next page**

***Figure 9: Dual AAV-hMYO7A reconstitutes hMYO7A and rescue retinal defects in sh1$^{-/-}$ mice*** (from Trapani *et al.*, 2014)

**(A)** Quantification of hMYO7A levels expressed from dual AAV-h*MYO7A* in subretinally injected sh1$^{-/-}$ eyecups. Levels of hMYO7A are reported as % of murine Myo7A expression in sh1$^{+/-}$. Sh1$^{-/-}$ untreated eyes do not express murine Myo7A. The number (n) of analyzed eyes are depicted below each bar. The quantification was performed by Western blot analysis using the anti-MYO7A antibody and measurements of MYO7A band intensities normalized to Dysferlin. The mean value is depicted above the corresponding bars. Values are represented as mean ± standard error of the mean (SEM).

**(B)** Representative pictures of analysis of correctly localized melanosomes to the RPE apical villi / 100 μm RPE. Arrows point at correctly localized melanosomes. Black scale bar = 10 μm.

**(C)** Quantification of correctly localized melanosomes in the RPE of sh1 following sub-retinal delivery of dual AAV-h*MYO7A*. The quantification is depicted as number of apical melanosomes/100 μm, the mean value is depicted above the corresponding bar. Values are presented as mean ± standard error of mean (SEM). The number (n) of analyzed eyes are depicted below each bar. **P ANOVA < 0.001. +/+: sh1$^{+/+}$; +/-: sh1$^{+/-}$; -/-: sh1$^{-/-}$; neg: eyes injected with AAV vectors expressing either 5'- or 3'- half of the dual AAV-h*MYO7A*; AK-*MYO7A*: dual AAV-h*MYO7A*

**(D)** Quantification of rhodopsin levels at the PR connecting cilium of sh1 following subretinal delivery of dual AAV-h*MYO7A*. The quantification is depicted as the mean number of rhodopsin coupled with gold particles per length of connecting cilium, the mean value is depicted above the corresponding bar. Values are represented as mean ± standard error of the mean (SEM). The n of eyes and connecting cilia analyzed is depicted below each bar. +/+: sh1$^{+/+}$; +/-: sh1$^{+/-}$; -/-: sh1$^{-/-}$; neg: eyes injected with AAV vectors expressing either 5'- or 3'- half of the dual AAV-h*MYO7A*; AK-*MYO7A*: dual AAV-h*MYO7A*.

## AIMS

**The overall aim of my project was to design gene therapy approaches for the treatment of rare recessive blinding diseases and to obtain pre-clinical data that will allow translation of adeno-associated viral (AAV)-mediated gene therapy strategies to the human eye**.

**The first aim of my project was to develop and test a gene therapy approach for gyrate atrophy of the choroid and retina (GA)** using an AAV vector strategy to deliver a correct copy of the disease causative gene, *ornithine amino-transferase* (*OAT*). As *OAT* is expressed almost ubiquitously, a 3XFlag-tagged human *OAT* (h*OAT*-3XFlag) plasmid was tested *in vitro* for expression and enzymatic activity upon transfection in HeLa and hARPE-19 cell lines. Following this, an AAV bearing the h*OAT*-3XFlag construct (AAV-h*OAT*-3XFlag) was subretinally injected in wild type mice and the biological potency of the vector was confirmed. AAV-h*OAT*-3XFlag was subretinally injected in the $Oat^{tm1DVa}$ ($Oat^{-/-}$) mouse, a model of GA, to assess rescue of retinal defects using clinically relevant ocular techniques at several time-points.

**The second aim was to translate a dual AAV approach to treat patients of Usher syndrome type 1B (USH1B) retinitis pigmentosa.** First, we designed dual AAVs carrying a long expression cassette for the disease causative gene, namely human *Myosin 7A* (h*MYO7A*). On discovery of a contaminant vector, specifically generated in the preparation of the AAV vector encoding the 5' half of h*MYO7A* (AAV-5'h*MYO7A*), we then proceeded with AAV design optimization. Once the vector design was finalized, I assessed the *in vivo* safety of a custom formulation buffer to avoid aggregation of dual AAV-h*MYO7A*.

As part of the pre-clinical studies, I developed an assay to evaluate the transgene-related potency of dual AAV-h*MYO7A* in sh1 mice, a relevant mouse model of USH1B; this assay is performed to ensure the biological potency and stability over time of dual AAV-h*MYO7A* that will be used in patients. Since this project represents a first use in humans for dual AAV-h*MYO7A*, I selected three doses of dual AAV-h*MYO7A* showing dose-dependent beneficial effects on sh1 mice retinal defects. These doses will be translated to USH1B subjects in the clinical trial.

# MATERIALS AND METHODS

### Generation of adeno-associated viral vector plasmids

The plasmids used for adeno-associated viral (AAV) vector production contain the inverted terminal repeats (ITRs) of AAV serotype 2.

The AAV vector plasmid required to generate AAV-human *ornithine aminotransferase* (h*OAT*) contains a cytomegalovirus (CMV) promoter and a chimeric promoter intron composed of the 5′ donor site from the first intron of the human β-globin gene and the branch and 3'-acceptor site from the intron of an immunoglobulin gene heavy chain variable region [92] followed by the human *OAT* coding sequence (CDS, NM_000274.4) with or without a 3XFlag tag at the C-terminal of the protein; the expression cassette is completed with the Woodchuck hepatitis virus post-transcriptional regulatory element (WPRE) and the bovine growth hormon polyA (BGH polyA).

The two AAV vector plasmids (5' and 3') required to generate dual AAV vectors contained several elements. The 5' plasmid contained a modified version of the CMV early enhancer/chicken β actin promoter (CAG) is composed of the CMV enhancer and a shorter version of the chicken beta-actin (CBA) promoter. We also added a promoter intron, either the chimeric intron or a modified version of the simian virus 40 promoter's intron (SV40) [93] followed by the N-terminal portion of the human *Myosin 7A* (h*MYO7A*) and a splice donor (SD) sequence. The 3' plasmid contained a splice acceptor sequence (SA) and the C-terminal portion of the transgene CDS followed by the BGH polyA. The h*MYO7A* CDS was split at a natural exon-exon junction, between exons 24-25 (5' half: NM_000260.3, bp 273-3380; 3' half: NM_000260.3, bp 3381-6920). For some experiments, a 3'-h*MYO7A* with the 3XFlag-tag at the C-terminal end was used. The splice donor (SD) and splice acceptor (SA) sequences contained in dual AAV vector plasmids are as follows:

5'-
GTAAGTATCAAGGTTACAAGACAGGTTTAAGGAGACCAATAGAAACTGGGCTTGTCGAGACAGA
GAAGACTCTTGCGTTTCT-3';

SA: 5'-GATAGGCACCTATTGGTCTTACTGACATCCACTTTGCCTTTCTCTCCACAG-3'.

The recombinogenic sequence contained in hybrid AK vector plasmids is derived from the phage F1 genome (Gene Bank accession number: J02448.1; bp 5850-5926). The AK sequence is:

5’-GGGATTTTGCCGATTTCGGCCTATTGGTTAAAAAATGAGCTGATTTAACAAAAATTTAACGCGA ATTTTAACAAAAT-3’.

The enhanced green fluorescent protein (EGFP) plasmids used in some experiments are as follows. The CAG promoter described above was coupled with either the chimeric intron or the modified version of the SV40 intron, followed by the EGFP sequence. The expression cassette is completed with the WPRE sequence and the BGH polyA.

**AAV vector production and characterization**

The AAV-h*OAT* vector was produced by InnovaVector while the dual AAV-h*MYO7A* vectors were produced by the TIGEM AAV Vector Core and by Reithera S.R.L. Vectors were produced by triple transfection of either HEK293 or HEK293T cells for AAV-h*OAT* and dual AAV-h*MYO7A*, respectively, followed by two rounds of CsCl2 purification [94]–[98]. Dual AAV-h*MYO7A* used in this work were produced under good manufacturing (GMP)-like practices, representative of the GMP production process that generated the clinical lot that will be used to treat subjects affected by Usher syndrome type 1B (USH1B). AAV-h*OAT* formulation buffer is composed of phosphate buffer saline (PBS, Thermo Fisher Scientific, Waltham, Massachusetts) + 5% glycerol. Dual AAV-h*MYO7A* were resuspended in a custom formulation buffer composed of PBS + 35 mM sodium chloride + 0.001% poloxamer 188 (P188, Sigma-Aldrich, St. Louis, Missouri) For each viral preparation, physical titers [genome copies (GC)/ml] were determined by TaqMan quantitative PCR (Applied Biosystems, Carlsbad, CA, USA). Primers and probes were designed to anneal on BGH pA for AAV-h*OAT* and AAV-3’h*MYO7A* or on 5’-h*MYO7A* for AAV-5’h*MYO7A*. The titer of AAV-h*OAT* was achieved by averaging the Taqman PCR on BGHpA with a dot-blot analysis on CMV promoter. AAV-5’h*MYO7A* and AAV-3’h*MYO7A* were separately filtered, titered and mixed by Reithera, then filtered and titered again. The alkaline Southern blot analysis for AAV-5’h*MYO7A* was carried out as follows: 3E+10 GC of viral DNA were extracted from AAV particles. To digest unpackaged genomes, the vector solution was incubated with 1 U/µL of DNase I (Roche, Milan, Italy) in a total volume of 300 µL containing 40 mM Tris–HCl, 10 mM NaCl, 6 mM MgCl2, 1 mM CaCl2 pH 7.9 for 2 h at 37°C. The DNase I was then inactivated with 50 mM EDTA, followed by incubation with proteinase K and 2.5% N-lauroyl-sarcosil solution at 50°C for 45 min to lyse the capsids. The DNA was extracted twice with phenol-chloroform and precipitated with two volumes of absolute ethanol and 10% sodium acetate (3 M, pH 7). Purified DNA was run in an alkaline agarose gel and imaged using the Digoxigenin non-radioactive method (Roche, Milan, Italy). One hundred ng of plasmid AAV-

5'h*MYO7A* was used as control. Ten µL of the 1 kb DNA ladder (N3232L; New England Biolabs, Ipswich, MA, USA) were loaded as molecular weight marker. The southern blot probe was obtained by enzymatic digestion of plasmid AAV-5'h*MYO7A* DNA using KpnI-XhoI to extract and purify a 544 base pair probe.

**Cell culture and transfection**

HEK293 and HeLa cells were maintained in Dulbecco's Modified Eagle Medium (DMEM) supplemented with 10% fetal bovine serum (FBS) (Thermo Fisher Scientific) while hARPE-19 cells were maintained in F12 medium supplemented with 10% FBS. For experiments of specific aim 1, cells were plated in 10 cm dishes (HeLa 3,6E+6 cells/dish, hARPE-19 4,8E+6 cells/dish, HEK293 3E+6 cells/dish). To transfect cells, medium was replaced 24 hours later with 3 mL of fresh pre-heated medium + 10 µg of plasmids diluted in lipofectamine LTX (Thermo Fisher Scientific). After an over-night incubation, cells received 7 mL of fresh pre-heated medium. Cells were harvested and lysed 72 hours post-transfection. For experiments of specific aim 2, HEK293 cells were plated in 6-well plates (1E+6 cells/well) and, 24 hours later, cells were transfected with 1.5 µg of plasmids diluted in calcium phosphate. After 4 hours, media was replaced with 2 mL of fresh pre-heated medium. Cells were harvested and lysed 72 hours post-transfection.

**Animal models**

Mice were housed at the TIGEM animal house (Pozzuoli, Italy) and maintained under a 12-h light/dark cycle (10–50 lux exposure during the light phase). $Oat^{tm1DVa/tm1DVa}$ (referred to as $Oat^{-/-}$) and pigmented $shaker1^{4626SB/4626SB}$ (referred to as $sh1^{-/-}$) mice were born by breeding heterozygous females with heterozygous males. Oat and sh1 mice used in this study were either affected ($Oat^{-/-}$, $sh1^{-/-}$) or unaffected ($Oat^{+/-}$, $sh1^{+/-}$). $Oat^{tm1DVa/tm1DVa}$ mice were generated by inserting the neomycine cassette in exon 3 of the murine Oat which leads to a frameshift and an early stop codon [13] thus murine Oat is not expressed. The genotype for $Oat^{tm1DVa}$ allele was performed by PCR analysis of genomic DNA extracted from mouse fingertip. The primers used for the PCR amplification are as follows: Fw (5'-AACTAGCAAGTCTGCAGACC-3') and Rev (5'-TCCACAAGGCATTCAGTGCG-3'), which generate a product of 290 bp for the wild type allele and a product of 1658 bp for the tm1DVa allele. $Oat^{-/-}$ pups die because of hypoargininemia-hyperammonemia; for this reason, pups were intraperitoneally injected twice a day from post-natal day (p) 1 to p15 with a solution 2:1 of 1M hydrochloride arginine and 1M arginine base (arginine final

concentration 1M pH ∽9); mice were injected with 10-15 µmol/gr of body weight and volume of injection was maintained constant so that final dose tapered to ∽2-5 µmol/gr of body weight during mice growth.

Shaker1$^{4626SB/4626SB}$ were generated by chemical mutagenesis resulting in an early non-sense mutation in the *Myo7A* gene thus the protein is not expressed [99]. Shaker1$^{4626SB/4626SB}$ present with clear hearing and vestibular defects, resulting in circling behaviour and loss of balance, but they do not show frank retinal degeneration possibly due to interspecies retinal differences [33]. The genotype for the *Myo7A$^{4626SB}$* allele was performed by PCR analysis of genomic DNA extracted from mouse fingertip followed by Sanger sequencing. The primers used for the PCR amplification are as follows: Fw (5'-GTGGAGCTTGACATCTACTTGACC-3') and Rev (5'-AGCTGACCCTCATGACTCTGC-3'), which generate a product of 712 bp that was sequenced with the Fw primer.

**Subretinal injection of AAV vectors in mice**

This study was carried out in accordance with the Association for Research in Vision and Ophthalmology Statement for the Use of Animals in Ophthalmic and Vision Research and with the Italian Ministry of Health regulation for animal procedures (Oat mice authorization n° 860/2020-PR; sh1 mice authorization n° 301/2020-PR). Surgery was performed under anesthesia and all efforts were made to minimize suffering. Adult mice were anesthetized with an intraperitoneal injection of 2 mL/100 g body weight of ketamine/medetomidine. An equal volume (1 or 1.1 µL) of either vector solution or excipient were delivered subretinally via a posterior trans-scleral trans-choroidal approach as described in [100].

**Retinal electrophysiology**

For electroretinographic analysis, mice were dark-adapted for 3 hours, anesthetized and positioned in a stereotaxic apparatus under dim red light. Their pupils were dilated with a drop of 0.5% tropicamide (Visufarma, Rome, Italy), and body temperature was maintained at 37°C. Light flashes were generated by a Ganzfeld stimulator (CSO, Costruzione Strumenti Oftalmici, Florence, Italy). The electrophysiological signals were recorded through gold-plate electrodes inserted under the lower eyelids in contact with the cornea. The electrodes in each eye were referred to a needle electrode inserted subcutaneously at the level of the corresponding frontal region. The different electrodes were connected to a two-channel amplifier. After completion of responses obtained in dark-adapted conditions (scotopic), the recording session continued with the purpose of dissecting the cone

pathway mediating the light response (photopic). To minimize the noise, different responses evoked by light were averaged for each luminance step. The maximal scotopic response of rods and cones was measured in dark conditions with two flashes of 0.7 Hz and a light intensity of 20 cd.s/m2, photopic cone responses were isolated in light conditions with a continuous background white light of 50 cd s/m2, with 10 flashes of 0.7 Hz and a light intensity of 20 cd.s/m2.

**Spectral-Domain Optical Coherence Tomography**

Spectral domain optical coherence tomography (SD-OCT) images were obtained using the Bioptigen Spectral Domain Ophthalmic Imaging System (SDOIS; Envisu R2200, Bioptigen, Morrisville, NC, USA). Mice were anesthetized and pupils were dilated by applying 1–2 drops of topical 0.5% tropicamide (Visufarma, Rome, Italy). To prevent corneal desiccation during the procedure, topical lubricant eye drops (Recugel; Bausch & Lomb, Rochester, NY, USA) were applied bilaterally with a small brush. Mice were positioned into the animal imaging mount and rodent alignment stage (AIM-RAS; Bioptigen, Morrisville, NC, USA); the laser source was placed in front of the mouse, and images were acquired by the InVivoVue Clinic software (Bioptigen, Morrisville, NC, USA). Three images, one central, one superior, and one inferior to the optic nerve, were taken from the temporal side and the nasal side of each eye. ONL thickness was manually measured three times from each OCT scan image and averaged.

**Western blot analysis**

Cells and eyecups (cups + retinas) for Western blot (WB) analysis were lysed in a custom buffer (50 mM Tris-HCl pH 7.4, 100 mM NaCl, 0,2 mM EDTA, 0,5% Triton) for OAT protein or RIPA buffer (50 mM Tris–HCl pH 8.0, 150 mM NaCl, 1% NP40, 0.5% Na-Deoxycholate, 1 mM EDTA pH 8.0, 0.1% SDS) for MYO7A protein. Both lysis buffers were supplemented with 0,5% phenylmethylsulfonyl fluoride (PSMF) (Sigma-Aldrich) and 1% complete EDTA-free protease inhibitor cocktail (Roche, Milan, Italy). Protein concentration was determined using Pierce BCA protein assay kit (Thermo-Scientific). After lysis, samples were denatured at 99°C for 5 min in 4X Laemmli sample buffer (Bio-rad, Milan, Italy) supplemented with ß-mercaptoethanol (Sigma-Aldrich) diluted 1:10. Samples for OAT analysis were separated on 12% SDS-polyacrilamide electrophoresis home-made gel, samples for MYO7A analysis on 4-20% gradient pre-cast TGX gels (Bio-rad). The following antibodies were used for

immuno-blotting: anti-OAT (1:1000, polyclonal, ab137679; Abcam, Cambridge, UK) that recognizes a peptide corresponding to aminoacids 30–395 of the hOAT protein (TKKTVQGPPTSDDIFEREYKYGAHNYHPLPVALERGKGIYLWDVEGRKYFDFLSSYSAVNQGHCHPKI VNALKSQVDKLTLTSRAFYNNVLGEYEEYITKLFNYHKVLPMNTGVEAGETACKLARKWGYTVKGIQK YKAKIVFAAGNFWGRTLSAISSSTDPTSYDGFGPFMPGFDIIPYNDLPALERALQDPNVAAFMVEPIQ GEAGVVVPDPGYLMGVRELCTRHQVLFIADEIQTGLARTGRWLAVDYENVRPDIVLLGKALSGGLYP VSAVLCDDDIMLTIKPGEHGSTYGGNPLGCRVAIAALEVLEEENLAENADKLGIILRNELMKLPSDVVT AVRGKGLLNAIVIKETKDWDAWKVCL; underlined aminoacids are different (8,2%) in murine Oat);

anti-3XFlag (1:1000, monoclonal, A8592; Sigma-Aldrich); custom anti-hMYO7A (1:200, polyclonal; Primm Srl, Milan, Italy) that recognizes a peptide corresponding to aminoacids 941–1070 of the hMYO7A protein (DMVDKMFGFLGTSGGLPGQEGQAPSGFEDLERGRREMVEEDLDAALPLPDEDEEDLSEYKFAKFAA TYFQGTTTHSYTRRPLKQPLLYHDDEGDQLAALAVWITILRFMGDLPEPKYHTAMSDGSEKIPV; underlined aminoacids are different (1,6%) in murine Myo7A); anti-Tubulin (1:1000, T9026, Sigma-Aldrich); anti-Calnexin (1:2000, ADI-SPA-865, Enzo Life Sciences, Farmingdale, New York, USA); anti-Dysferlin (1:500, MONX10795; Tebu-bio, Le Perray-en-Yveline, France). The quantification of WB bands was performed using ImageJ software. hOAT and hMYO7A expression was normalized over the expression of one of the house-keeping genes, depending on cell or tissue type and molecular weight.

**OAT activity assay**

OAT activity was measured in cells and eyecups with the ninhydrin method previously described in [101]. Samples were lysed in a custom buffer (50 mM Tris-HCl pH 7.4, 100 mM NaCl, 0,2 mM EDTA, 0,5% Triton) supplemented with 0,5% PSMF (Sigma-Aldrich) and 1% complete EDTA-free protease inhibitor cocktail (Roche). Protein concentration was determined using Pierce BCA protein assay kit (Thermo-Scientific). Then, 100 µg of protein lysate was added to the reaction mix composed of 50 mM Tris-HCl pH 8, 35 mM L-ornithine hydrochloride (Sigma-Aldrich), 5 mM α-ketoglutarate (Sigma-Aldrich), 0.05 mM pyridoxal phosphate (Sigma-Aldrich) (final volume 1 mL). The reaction was incubated 10 minutes at room temperature (RT), then 0,5h at 37°C. Reaction was stopped by adding 250 µL of 3.6N perchloric acid (Sigma-Aldrich) and inverting tubes 6-8 times, then 250 µL of 2% ninhydrin (Sigma-Aldrich) were added and tubes were inverted 6-8 times. Ninhydrin complexes were allowed to form at 99°C for 15', then tubes were centrifuged 10' at 2500 G at RT.

Supernatant was decanted and complexes were resuspended in 500 µL ethanol. Each sample was read in duplicate using an absorbance wavelength of 490 nm.

**Melanosome localization analysis**

Eyes from pigmented sh1 mice (+/- or -/-) were enucleated 3 months following the AAV injection and cauterized on the temporal side of the cornea. Fixation was performed using 2% glutaraldehyde-2% paraformaldehyde in 0.1 M PBS overnight, rinsed in 0.1 M PBS and dissected under a light microscope. The temporal portions of the eyecups were embedded in Araldite 502/ EMbed 812 (Araldite 502/EMbed 812 KIT, catalog #13940; Electron Microscopy Sciences, Hatfield, PA, USA). Semi-thin (0.5 µm) sections were transversally cut on a Leica Ultramicrotome RM2235 (Leica Microsystems, Bannockburn, IL, USA), mounted on slides and stained with toluidine blue and borace staining. Melanosomes were counted by a masked operator in a montage of the entire retinal section obtained through acquisition of overlapping fields using a Zeiss Apotome (Carl Zeiss, Oberkochen, Germany) with 100X magnification; then, the entire retinal section was reconstituted on Photoshop software (Adobe, San Jose, California). Melanosomes count and retinal pigment epithelium (RPE) measurements were performed using ImageJ software. Melanosome number was normalized over the length of the RPE divided by 100 µm.

**Statistical analysis**

The Student's t-test was used to compare data depicted in **Figure 13, 19, 20**. **Figure 13, AAV-hOAT-3XFlag activity in subretinally injected C57BL/6 mice**: the p-value between C57BL/6 eyes treated with AAV-CMV-hOAT-3XFlag-WPRE-BGH Vs formulation buffer is 0,214. **Figure 19, *in vivo* comparison of chimeric intron and SV40 intron**: the p-value between C57BL/6 eyes treated with dual AAV-Chimeric intron-*MYO7A*-3XFlag Vs dual AAV-SV40 intron-*MYO7A*-3XFlag is 0,410. **Figure 20A, safety of dual AAV formulation 14 days post-injection at ERG**: the p-values between C57BL/6 eyes treated with PBS + 35 mM NaCl + 0,001% PF68 formulation buffer Vs regular formulation buffer are the following. Log -4 cd.s/m2, A-wave = 0,519; B-wave = 0,468. Log -1,6 cd.s/m2, A-wave = 0,815; B-wave = 0,720. Log -1 cd.s/m2, A-wave = 0,519; B-wave = 0,474. Log -0,3 cd.s/m2, A-wave = 0,967; B-wave = 0,765. Log 0 cd.s/m2, A-wave = 0,361; B-wave = 0,671. Log 1 cd.s/m2, A-wave = 0,893; B-wave = 0,767. Log 1,3 cd.s/m2, A-wave = 0,804; B-wave = 0,298. Photopic, A-wave = 0,575; B-wave = 0,689. **Figure 20B, safety of dual AAV formulation 28 days post-injection at ERG**: the p-values between C57BL/6 eyes treated with PBS + 35 mM NaCl + 0,001% PF68

formulation buffer Vs regular formulation buffer are the following. Log -4 cd.s/m2, A-wave = 0,643; B-wave = 0,256. Log -1,6 cd.s/m2, A-wave = 0,641; B-wave = 0,876. Log -1 cd.s/m2, A-wave = 0,597; B-wave = 0,910. Log -0,3 cd.s/m2, A-wave = 0,634; B-wave = 0,854. Log 0 cd.s/m2, A-wave = 0,727; B-wave = 0,551. Log 1 cd.s/m2, A-wave = 0,960; B-wave = 0,909. Log 1,3 cd.s/m2, A-wave = 0,398; B-wave = 0,617. Photopic, A-wave = 0,811; B-wave = 0,710. **Figure 20C, safety of dual AAV formulation 16 and 35 days post-injection at OCT**: the p-values between C57BL/6 eyes treated with PBS + 35 mM NaCl + 0,001% PF68 formulation buffer s regular formulation buffer are 0,287 at 16 days post-injection and 0,574 at 35 days post-injection.

One-way analysis of variance (ANOVA) followed by Tuckey post-hoc analysis was used to perform multi pairwise comparisons between groups in **Figure 11 and 23. Figure 11, similar activity between hOAT and hOAT-3XFlag activity *in vitro***: the ANOVA p-values are the following. Untransfected HEK293 Vs either HeLa pEGFP (pANOVA < 0,001), HeLa pOAT (pANOVA < 0,001), HeLa pOAT-3XFlag (pANOVA < 0,0001), hARPE-19 pEGFP (pANOVA < 0,001), hARPE-19 pOAT (pANOVA = 0,062) or hARPE-19 pOAT-3XFlag (pANOVA < 0,01); HeLa pEGFP Vs either HeLa pOAT (p-value < 0,0001), HeLa pOAT-3XFlag (pANOVA < 0,0001), hARPE-19 pEGFP (pANOVA = 0,943), hARPE-19 pOAT (pANOVA < 0,0001) or hARPE-19 pOAT-3XFlag (pANOVA < 0,0001); HeLa pOAT Vs either HeLa pOAT-3XFlag (pANOVA = 0,968), hARPE-19 pEGFP (pANOVA < 0,0001), hARPE-19 pOAT (pANOVA = 0,116) or hARPE-19 pOAT-3XFlag (pANOVA = 0,941); HeLa pOAT-3XFlag Vs either hARPE-19 pEGFP (pANOVA < 0,0001), hARPE-19 pOAT (pANOVA < 0,05) or hARPE-19 pOAT-3XFlag (pANOVA = 0,506); hARPE-19 pEGFP Vs either hARPE-19 pOAT (pANOVA < 0,0001) or hARPE-19 pOAT-3XFlag (pANOVA < 0,0001); hARPE-19 pOAT Vs hARPE-19 pOAT-3XFlag (pANOVA = 0,506). **Figure 23, dose-dependent effects on correctly localized melanosomes to the retinal pigment epithelium**: the ANOVA p-values are the following. Affected $sh1^{-/-}$ injected with formulation buffer Vs either unaffected $sh1^{+/-}$ injected with formulation buffer (pANOVA < 0,0001), $sh1^{-/-}$ treated with the high dose (pANOVA < 0,0001), $sh1^{-/-}$ treated with the medium dose (pANOVA <0,01) or $sh1^{-/-}$ treated with the low dose (pANOVA = 0,313); $sh1^{-/-}$ treated with the high dose Vs either unaffected $sh1^{+/-}$ injected with formulation buffer (pANOVA = 0,105), $sh1^{-/-}$ treated with the medium dose (pANOVA = 0,113) or $sh1^{-/-}$ treated with the low dose (pANOVA < 0,01); $sh1^{-/-}$ treated with the medium dose Vs either unaffected $sh1^{+/-}$ injected with formulation buffer (pANOVA < 0,001) or $sh1^{-/-}$ treated with the low dose (pANOVA 0,442); unaffected $sh1^{+/-}$ injected with formulation buffer Vs $sh1^{-/-}$ treated with the low dose (pANOVA < 0,0001). Due to the

variability of sh1$^{+/-}$ injected with formulation buffer impacting the ANOVA analysis, comparisons were analyzed again without unaffected controls and the ANOVA p-values are the following: affected sh1$^{-/-}$ injected with formulation buffer Vs sh1$^{-/-}$ treated with the high dose (pANOVA < 0,0001), sh1$^{-/-}$ treated with the medium dose (pANOVA <0,0001) or sh1$^{-/-}$ treated with the low dose (pANOVA < 0,01); sh1$^{-/-}$ treated with the high dose Vs either sh1$^{-/-}$ treated with the medium dose (pANOVA < 0,001) or sh1$^{-/-}$ treated with the low dose (pANOVA < 0,0001); sh1$^{-/-}$ treated with the medium dose Vs sh1$^{-/-}$ treated with the low dose (pANOVA < 0,05).

ANOVA analysis followed by Dunn test and subsequently student t-test were used to compare data in **Figure 14**, **AAV-hOAT-3XFlag improves outer nuclear layer of Oat$^{-/-}$ mice**: the ANOVA p-values are the following: unaffected Oat$^{+/-}$ injected with formulation buffer Vs either Oat$^{-/-}$ treated with AAV-h*OAT*-3XFlag (pANOVA = 0,224) or Oat$^{-/-}$ injected with formulation buffer (pANOVA = 0,008); Oat$^{-/-}$ treated with AAV-h*OAT*-3XFlag Vs Oat$^{-/-}$ injected with formulation buffer (pANOVA = 0,639). The p-value between Oat$^{-/-}$ treated with AAV-h*OAT*-3XFlag Vs Oat$^{-/-}$ injected with formulation buffer is 0,026.

Data are presented as mean [± standard error of the mean (s.e.m.)] which has been calculated using the number of independent *in vitro* experiments or eyes (not replicate measurements of the same sample). Statistical p-values ≤ 0.05 were considered significant.

# RESULTS

## Aim 1: Gene therapy for gyrate atrophy of the choroid and retina

### Generation of human *ornithine aminotransferase*-3XFlag plasmid for adeno-associated vector production

The human *ornithine aminotransferase* (h*OAT*) coding sequence (CDS) is ∽ 1.3 Kb and can be efficiently packaged into a single adeno-associated viral (AAV) vector. Since the *OAT* gene is expressed almost ubiquitously, a version of h*OAT* tagged with a 3XFlag at the C-terminus was generated, which is easily discriminated from the endogenous protein. As previous studies reported that *OAT* is expressed both in retinal pigment epithelial (RPE) cells and photoreceptor (PRs) cells, the h*OAT*-3XFlag CDS was put under the control of a full-length ubiquitous cytomegalovirus (CMV) promoter (Fig. 10).


***Figure 10: Schematic representation of AAV-hOAT constructs***

Black hairpins: AAV serotype 2 inverted terminal repeats (ITRs); CMV: cytomegalovirus; promoter intron: chimeric intron; *OAT*-3XFlag: human *ornithine aminotransferase* coding sequence 3XFlag-tagged; WPRE: Woodchuck hepatitis virus post-transcriptional regulatory element; BGH PA: bovine growth hormone polyA.

### *Expression and activity of human ornithine aminotransferase in transfected cell lines*

The h*OAT*-3XFlag plasmid (hereafter referred to as p*OAT*-3XFlag) was tested for expression and enzymatic activity upon transfection into two cell lines with relatively low expression of hOAT, HeLa cells and hARPE19-cells (https://www.proteinatlas.org/ENSG00000065154-OAT/cell); HEK293 cells were used as positive control given their high levels of hOAT protein. Additionally, we performed a comparison between the h*OAT* plasmid (p*OAT*) and p*OAT*-3XFlag tagged to ensure that tag addition to the protein does not alter enzymatic activity. Western blot (WB) analysis on cell lysate transfected with p*OAT* showed over-expression of h*OAT* (∽45 KDa) while cells transfected with p*OAT*-3XFlag expressed both the endogenous h*OAT* and h*OAT*-3XFlag (∽48 KDa) (n of 3 independent experiments) (Fig. 11). As expected, low levels of hOAT are detectable in HeLa and hARPE-19 cells transfected with a plasmid encoding for the enhanced green fluorescent protein (pEGFP) (Fig. 11).

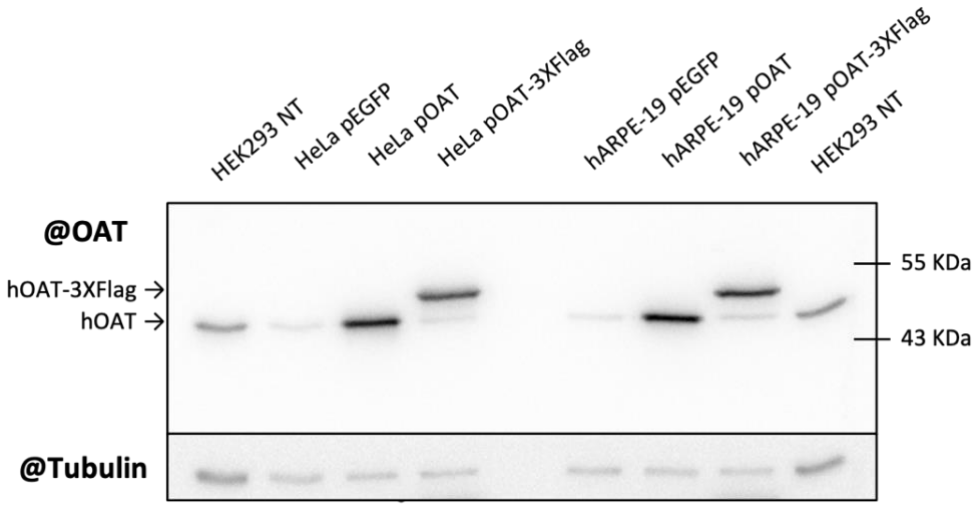


***Figure 11: Expression of hOAT in cell lines transfected with pOAT or pOAT-3XFlag***

Representative WB analysis of HeLa and hARPE-19 transfected with p*OAT* or p*OAT*-3XFlag. HeLa and hARPE-19 cells transfected with a plasmid encoding for EGFP were used as controls; non-transfected HEK293 cells were used as control cells with relatively high expression of OAT. Black bars correspond to 43 and 55 KDa, arrows indicate hOAT or hOAT-3XFlag, 10 µg of proteins were loaded in each lane. @OAT: WB with anti-Ornithine aminotransferase antibody; @Tubulin: WB with anti-Tubulin antibody, used as loading control; pEGFP: plasmid encoding for EGFP; p*OAT*: plasmid encoding for OAT; p*OAT*-3XFlag: plasmid encoding for OAT-3XFlag.

The same cell lysates were tested in an OAT activity assay based on the use of ninhydrin, which forms complexes with the OAT reaction product, pyrroline 5-carboxilate (P5C) [101] (Fig. 12A). Ninhydrin complexes form a red pigment in hot acidic conditions that precipitates in water, thus allowing absorbance to be measured at 490 nm wavelength. From the results, we detected a 4-5X significant increase of hOAT activity compared to the negative control, pEGFP, in HeLa cells (Fig. 12, p*OAT* or p*OAT*-3XFlag vs pEGFP, p-value < 0,0001) and hARPE-19 cells (Fig. 12, p*OAT* or p*OAT*-3XFlag vs pEGFP, p-value < 0,0001) upon transfection of either p*OAT* or p*OAT*-3XFlag. Both plasmids induced a 1,4-1,8X increase compared to our positive control, HEK293 cells (Fig. 12, HeLa p*OAT* vs HEK293, p-value < 0,001; HeLa p*OAT*-3XFlag vs HEK293, p-value < 0,0001; hARPE-19 p*OAT* vs HEK293, p-value = 0,062; hARPE-19 p*OAT*-3XFlag vs HEK293, p-value < 0,01). No significant difference in hOAT enzymatic activity was measured between p*OAT* and p*OAT*-3XFlag transfected cells in either cell line (HeLa cells, p-value = 0,968; hARPE19 cells, p-value = 0,506) [Fig. 12B, one-way analysis of variance (ANOVA) with Tuckey post-hoc analysis)]. More details on statistical analysis are provided in materials and methods.

As OAT is expressed in a wide range of tissues, we used p*OAT*-3XFlag to generate the AAV vector for *in vivo* experiments.

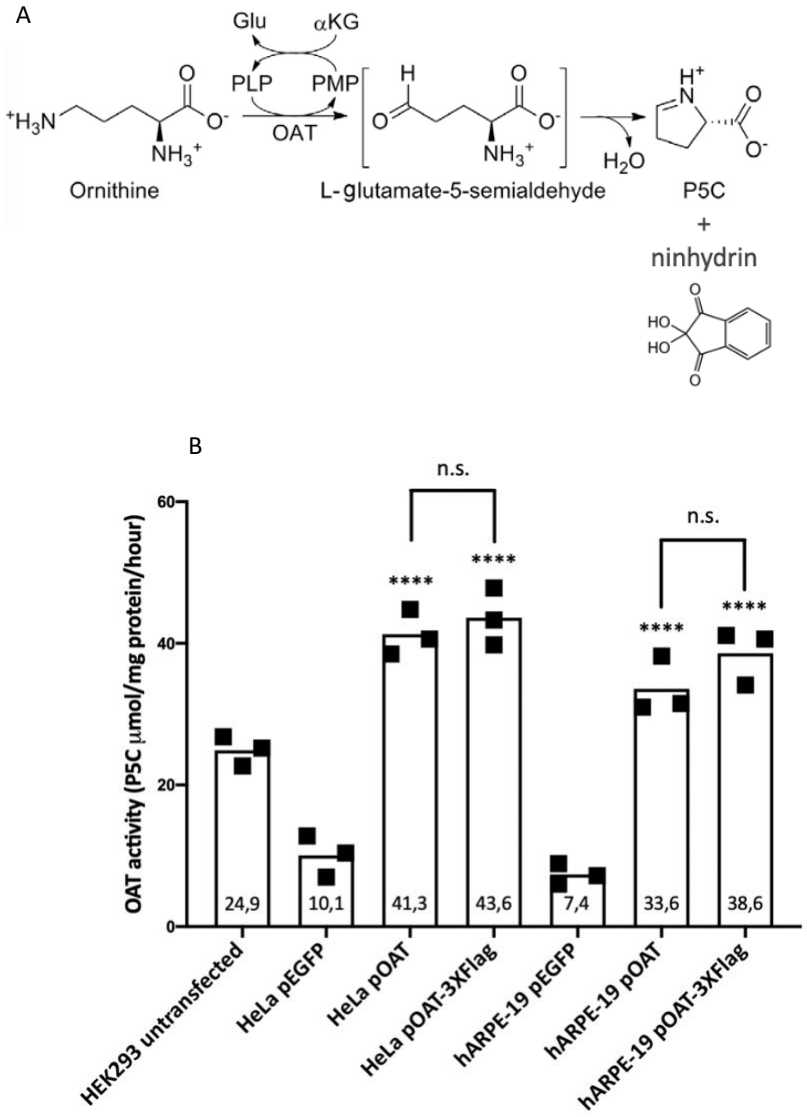


**For figure 12 caption see next page.**

***Figure 12: Plasmids encoding hOAT or hOAT-3XFlag significantly increases* OAT *activity***

**(A)** Scheme of OAT biochemical reaction to form pyrroline 5-carboxylate. Ninhydrin binds the amine group of pyrroline 5-carboxylate and forms a red precipitate that can be resuspended in ethanol to measure absorbance at 490 nm (modified from Juncosa *et al.*, 2013) [102]. Glu: glutamate; α-KG: α-ketoglutarate; PLP: pyridoxal 5'-phosphate; PMP: pyridoxamine-phosphate; P5C: pyrroline 5-carboxilate.
**(B)** Quantification of OAT activity with the ninhydrin method. HeLa cells and hARPE-19 cells were transfected with plasmids encoding for h*OAT*, h*OAT*-3XFlag or enhanced green fluorescent protein (EGFP) as a control with relatively low expression of OAT; non-transfected HEK293 cells were used as control cells with relatively high expression of OAT. One hundred µg of protein lysate were used per sample in the assay. Results are represented as value of each biological replicate (filled square) and as mean value for each group (column). Mean value of each group is indicated inside the corresponding bar. Statistical analysis was conducted using one-way ANOVA with Tuckey post-hoc analysis. Stars above each bar refer to the comparison between p*OAT* or p*OAT*-3XFlag vs pEGFP in the same cell line. P-values are: **** <0.0001; n.s.: no significant difference. P5C: pyrroline 5-carboxilate; pEGFP: plasmid encoding for EGFP; p*OAT*: plasmid encoding for *OAT*; p*OAT*-3XFlag: plasmid encoding for *OAT*-3XFlag.

## Sub-retinal administration of AAV-h*OAT*-3XFlag results in efficient transgene expression in mouse retina

Adult C57BL/6 mice were subretinally injected with AAV-CMV-h*OAT*-3XFlag-WPRE-BGHpA (AAV-h*OAT*-3XFlag) (dose 3.0E+9 genome copies (GC)/eye) to assess vector-induced transgene expression in the murine eye and to detect any increases in OAT activity. Four weeks post-injection, WB analysis was performed on whole eyecups and confirmed efficient expression of h*OAT*-3XFlag in 100% of eyes (8/8 eyes) injected with AAV-h*OAT*-3XFlag (Fig. 13).

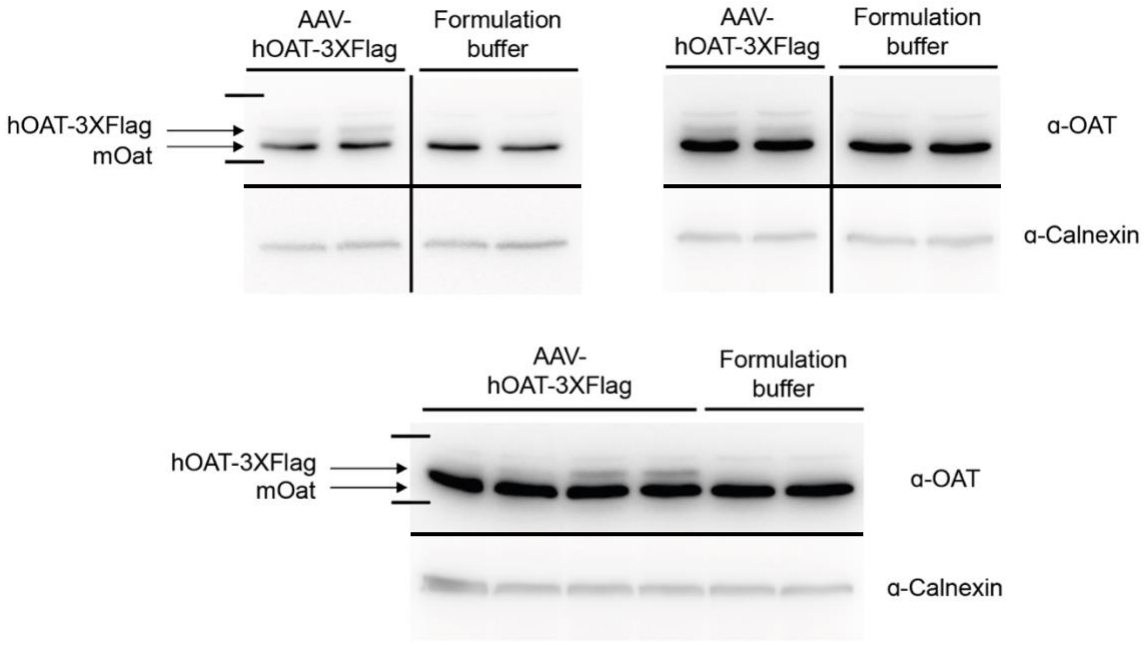


***Figure 13: Efficient expression of hOAT upon sub-retinal administration of AAV-hOAT-3XFlag in vivo***

WB analysis of C57BL/6 eyecups 4 weeks following subretinal injection of either AAV-h*OAT*-3XFlag or formulation buffer. Each image shows different eyecups samples, black bars correspond to 43 and 55 KDa, arrows indicate mOat or hOAT-3XFlag. Fifty µg of protein were loaded in each lane. α-OAT: western blot with anti-Ornithine aminotransferase antibody; α-Calnexin: western blot with anti-Calnexin antibody, used as loading control.

The same eyecups lysates were also evaluated for OAT activity. The ninhydrin assay shows no statistical difference between eyes injected with AAV-h*OAT*-3XFlag or formulation buffer (Fig. 14, two sample t-test statistical analysis, p-value = 0,214).

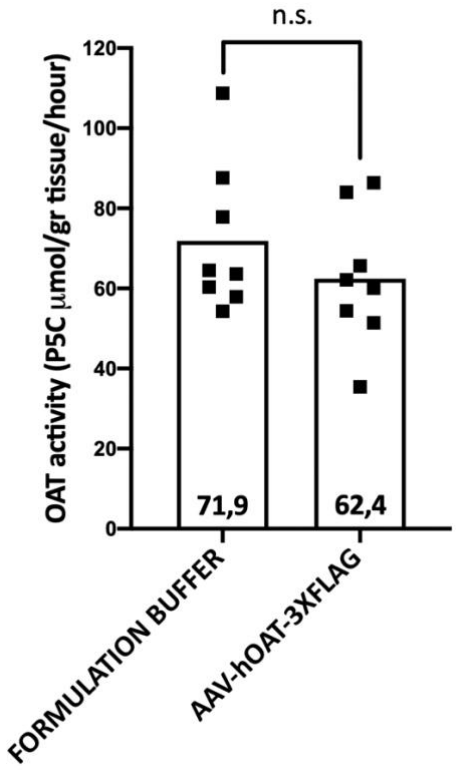


***Figure 14: OAT activity assay in eyecups of C57BL/6 mice injected subretinally with AAV-hOAT-3XFlag***

Quantification of OAT activity in eyecups of C57BL/6 mice subretinally injected with either AAV-h*OAT*-3XFlag or formulation buffer. One hundred µg of protein lysate were used per sample in the assay. Statistical analysis was conducted using two-sample t-test analysis. P5C: pyrroline 5-carboxilate; n.s.: no significant difference.

### AAV-h*OAT*-3XFlag rescues *Oat*$^{-/-}$ mice retinal defects

To assess retinal improvements of AAV-h*OAT*-3XFlag, we selected a GA mouse model lacking exon 3 of murine *Oat* (*Oat*$^{tm1DVa}$ or *Oat*$^{-/-}$), resulting in the absence of murine Oat expression. *Oat*$^{-/-}$ mice die in the neonatal stage of life due to hypoargininemia-hyperammonemia. To save knockout pups, we performed intraperitoneal injection of arginine (from pnd1 to pnd14, injections every 12 ± 3 hours). Electroretinogram (ERG) and histology analysis published in a previous study [13] showed that both retinal function and structure are preserved in *Oat*$^{-/-}$ mice up to 2 months of age, therefore we subretinally injected *Oat*$^{-/-}$ at 1 month of age. Each animal was injected with AAV-h*OAT*-3XFlag (dose 5.4E+9 GC/eye) in one eye while the contralateral eye received formulation buffer as negative control. *Oat*$^{+/-}$ mice were injected with formulation buffer as unaffected controls. Spectral domain-Optical coherence tomography (SD-OCT) analysis performed at an early timepoint of the disease (4 months of age) shows that AAV-h*OAT*-3XFlag increased outer nuclear layer (ONL) thickness in *Oat*$^{-/-}$ eyes compared to contralateral control eyes, which received the formulation buffer (14% increase) (Fig. 15). One-way ANOVA analysis

confirmed significant difference between unaffected *Oat*$^{+/-}$ eyes receiving the formulation buffer compared to affected *Oat*$^{-/-}$ untreated eyes (Fig. 15, pANOVA = 0,008) and no significant difference when comparing unaffected *Oat*$^{+/-}$ eyes and affected Oat$^{-/-}$ eyes subretinally injected with AAV-h*OAT*-3XFlag (Fig. 15, pANOVA = 0,224). However, there was no significant difference between affected *Oat*$^{-/-}$ eyes treated with AAV-h*OAT*-3XFlag and affected *Oat*$^{-/-}$ eyes receiving the formulation buffer (Fig. 15, pANOVA = 0,639). These two groups were compared again using the student t-test which showed statistical significance (Fig. 15, p-value = 0,026).

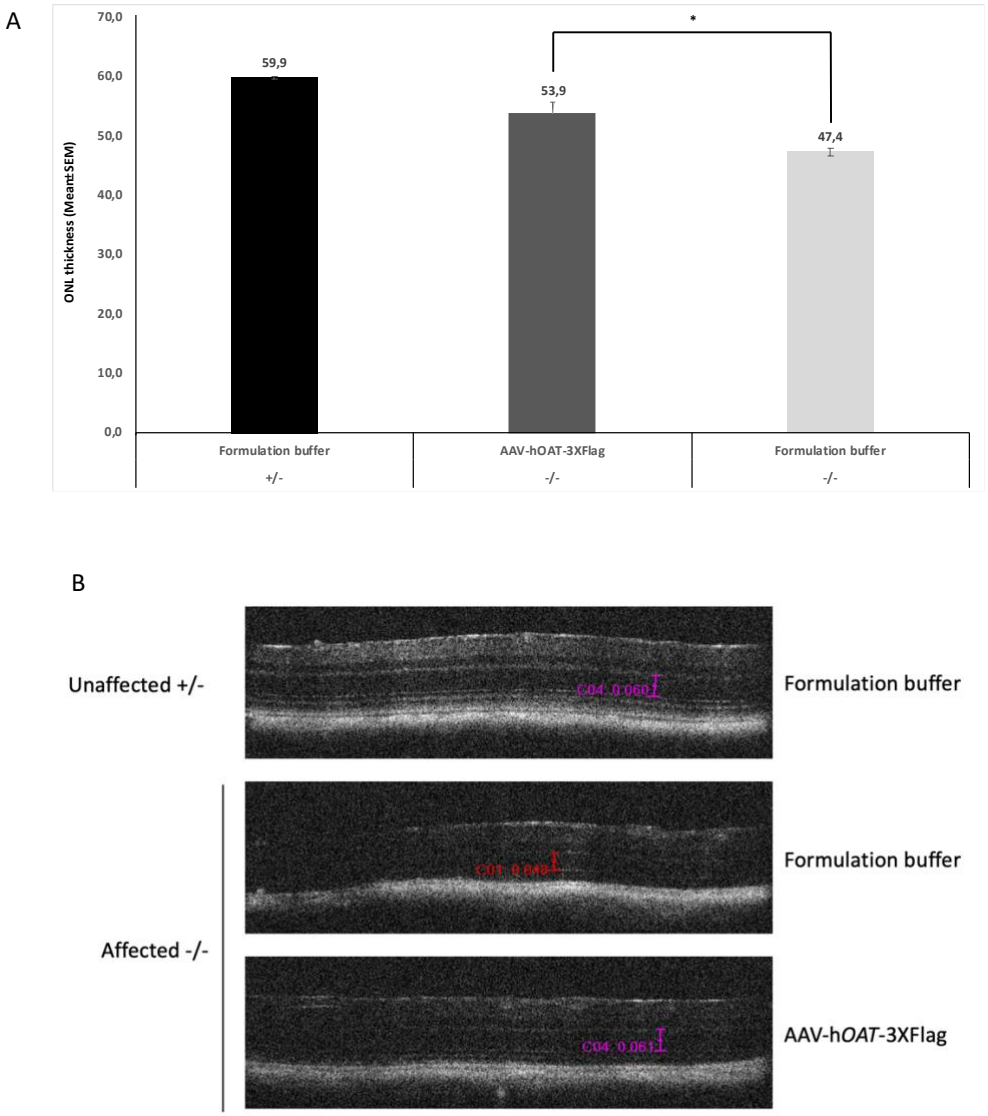


***Figure 15: AAV-hOAT-3XFlag improved outer nuclear layer thickness upon sub-retinal injection in Oat$^{-/-}$ mice.***

(**A**) SD-OCT analysis was performed at 4 months of age to measure the ONL thickness in *Oat*$^{-/-}$ mice injected sub-retina with either AAV-h*OAT*-3XFlag (dark grey bar, n = 4 eyes) or formulation buffer (light grey bar, n = 3 eyes) in the contralateral eye. Heterozygous (*Oat*$^{+/-}$) mice injected with formulation buffer were used as unaffected controls (dark bar, n = 8 eyes). For each eye, ONL thickness was measured close to the injection site and away from the injection site, then values were averaged. Results are represented as mean value for each eye (filled square) and as mean value for each group of treatment (column). Mean value of each group is indicated inside the corresponding bar. Statistical analysis was conducted using two-sample t-test analysis to evaluate significant differences between Oat$^{-/-}$ eyes treated with AAV-h*OAT*-3XFlag and Oat$^{-/-}$ eyes receiving formulation buffer. * p-value < 0,05. ONL: outer nuclear layer; +/- : heterozygous unaffected *Oat* mice; -/- : homozygous affected *Oat* mice.

(**B**) Representative retinal scannings of 4-month old unaffected heterozygous (*Oat*$^{+/-}$) mice injected with formulation buffer and affected homozygous (*Oat*$^{-/-}$) mice injected with AAV-h*OAT*-3XFlag or formulation buffer. Calipers for ONL measurements are either in red or magenta and show mm of retinal thickness. +/- : heterozygous unaffected *Oat* mice; -/- : homozygous affected *Oat* mice.

ERG analysis did not show functional improvement at 4 months of age of the retinal circuitry, measured both with the A-Wave (Fig. 16A) and the B-Wave (Fig. 16B) in *Oat*$^{-/-}$ eyes injected with AAV-h*OAT*-3XFlag compared to contralateral eyes injected with the formulation buffer. Further analysis at later time-points may reveal therapeutic effects on retinal function and retinal morphology.

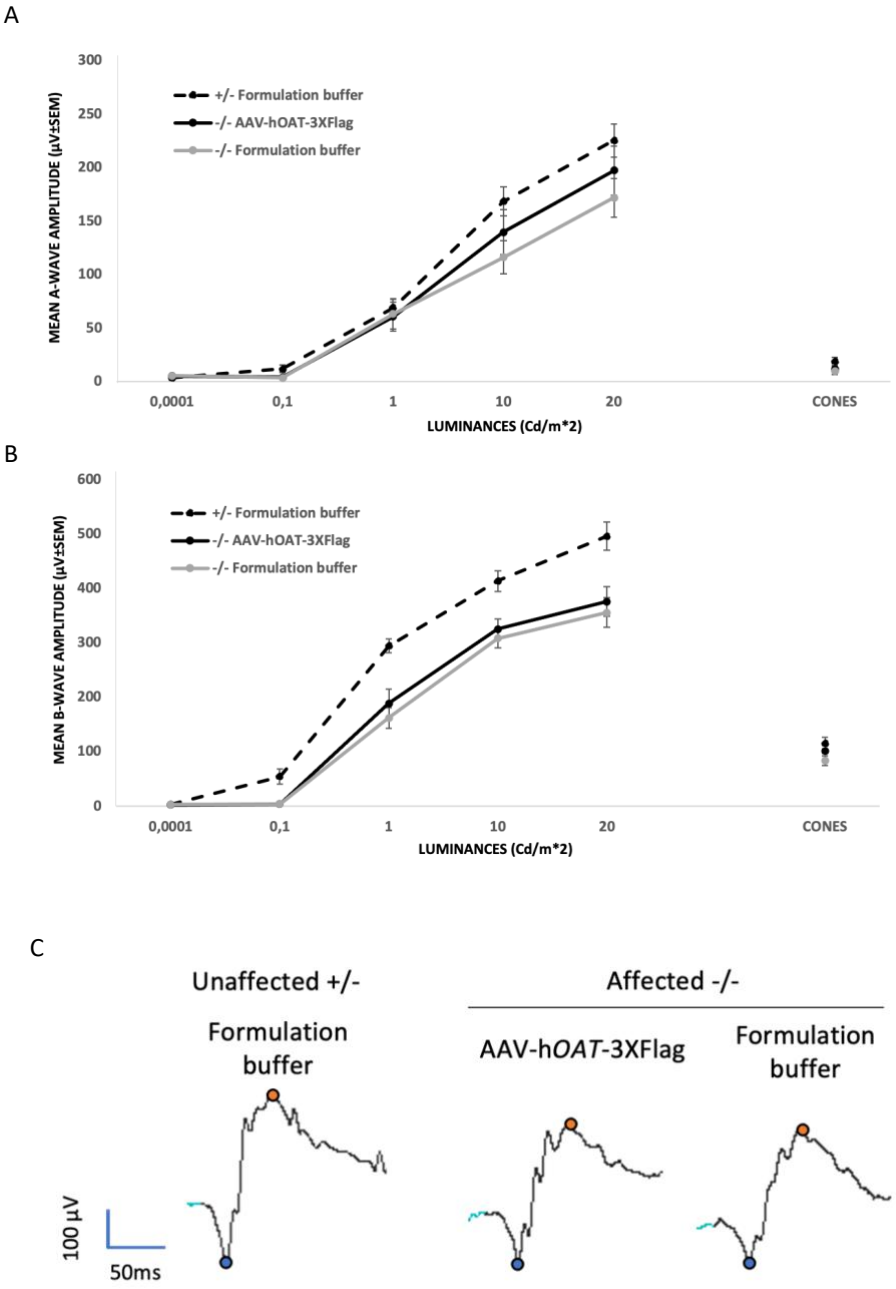


***Figure 16: AAV-hOAT-3XFlag improved retinal function in subretinally injected Oat$^{-/-}$ mice.***

Electroretinogram analysis to assess A-wave (**A**) and B-wave (**B**) was performed at 4 months of age in *Oat*$^{-/-}$ mice injected subretinally with either AAV-h*OAT*-3XFlag (black line, n of eyes = 5) or formulation buffer (grey line, n of eyes = 5) in the contralateral eye at 4 months of age. Heterozygous (*Oat*$^{+/-}$) mice injected with formulation buffer (dotted black line, n of eyes = 11) were used as unaffected controls. Mice eyes were stimulated with a luminance range from 0,0001 to 20 candelas/m$^2$. Data are represented as mean ± standard error of mean (SEM). Cd: candela; +/- : heterozygous unaffected *Oat* mice; -/- : homozygous affected *Oat* mice.

(**C**) Representative ERG waves at 20 cd/m*2 of 4 month-old unaffected heterozygous (*Oat*$^{+/-}$) mice injected with formulation buffer and affected homozygous (*Oat*$^{-/-}$) mice injected with AAV-h*OAT*-3XFlag or formulation buffer. Blue point indicates A-Wave, orange point indicates B-Wave. Vertical scale bar = 100 µV, horizontal scale bar = 50 ms. +/- : heterozygous unaffected *Oat* mice; -/- : homozygous affected *Oat* mice.

## Aim 2: Gene therapy for Usher syndrome type 1B Retinitis Pigmentosa

### Generation and sequencing of plasmids for dual AAV-human *Myosin7A* vector production

Plasmids for dual AAV-human *Myosin7A* (h*MYO7A*) were previously generated in our lab. Briefly, the expression cassette of h*MYO7A* is split into a 5'-half and a 3'-half, each cloned in a plasmid for AAV vector production. Bacterial resistance in the plasmid backbone was changed from ampicillin to kanamycin following the guidelines on clinical products from the regulatory authorities. Plasmids were then completely sequenced with the Sanger method. ITRs form a hairpin secondary structure that blocks sequencing, therefore ITRs were resolved by enzymatic restriction using BsaHI prior to sequencing. The promoter intron in AAV-5'h*MYO7A* was changed from the chimeric intron to a modified version of the Simian virus 40 (SV40) intron as explained in the next paragraph. For the experiment in figure 20, a 3'h*MYO7A* 3XFlag-tagged at the C-terminal was generated in the lab. A schematic representation of dual AAV-h*MYO7A* plasmids is reported in figure 17.

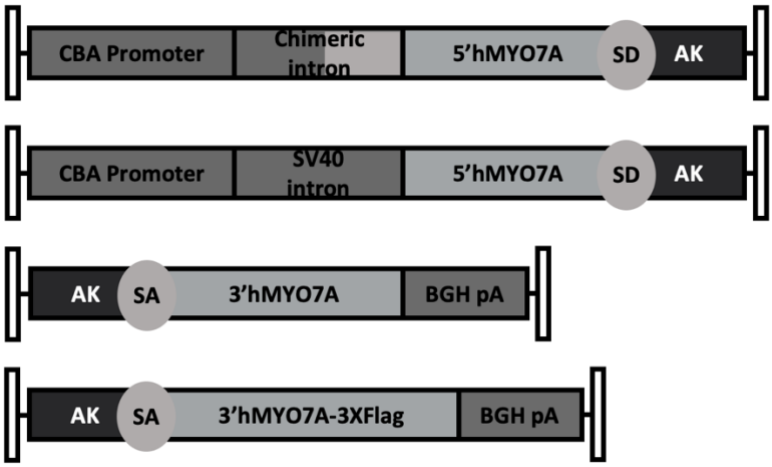


***Figure 17: Schematic representation of dual AAV-hMYO7A constructs***

Black hairpins: AAV serotype 2 ITRs; CBA: chicken beta-actin; 5'h*MYO7A*: 5' half of human *Myosin7A* coding sequence; AK: recombinogenic sequence from F1 phage; 3'h*MYO7A*: 3' half of human *Myosin7A* coding sequence; BGH PA: bovine growth hormone polyA; 3'h*MYO7A*-3XFlag: 3' half of human *Myosin7A* coding sequence 3XFlag-tagged.

### Optimization of AAV-5'h*MYO7A* to avoid a contaminant vector

During dual AAV-h*MYO7A* production for non-clinical studies in view of a clinical translation, we discovered a contaminant vector in the AAV-5'h*MYO7A* preparation. Southern blot (SB) analysis, developed using a probe that recognizes the Chicken beta-actin (CBA) promoter, showed a band of ∽4.5 kb corresponding to AAV-5'h*MYO7A* and an unexpected band of ∽ 1.3 Kb (Fig. 18A). We hypothesized that a homologous recombination event takes place due to an 82 base pair stretch of sequence similarity between the chimeric promoter intron and the splicing donor (SD) signal (Fig. 18B-C). This leads to deletion of the remaining portion of the intron and of the 5'h*MYO7A* sequence while the recombined DNA still retains AAV ITRs, thus supporting vector production (Fig. 18D). We were able to confirm the presence of this construct by subcloning and sequencing the purified viral DNA.

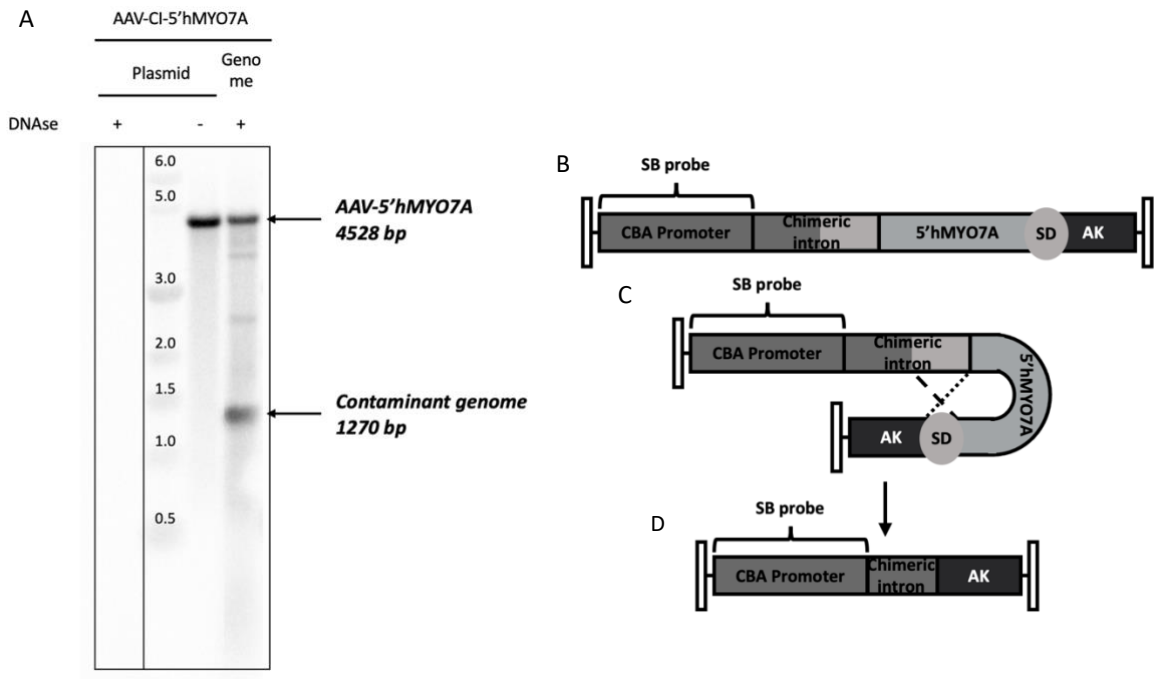


***Figure 18: A contaminant vector in the AAV-5'hMYO7A preparation***

(**A**) SB image showing genomes corresponding to the AAV-5'h*MYO7A* (indicated by the upper arrow) and to the contaminant vector (indicated by the lower arrow). The molecular weight marker is expressed in kilobases. DNAse: treatment with DNAse for degradation of contaminant external DNA; plasmid: plasmid DNA for production of AAV-5'h*MYO7A* bearing the chimeric intron (AAV-CI-5'h*MYO7A*); genome: genomic DNA extracted from AAV-CI-5'h*MYO7A*; bp: base pair.

(**B**) Schematic representation of AAV-5'h*MYO7A* vector; the sequence recognized by the SB probe is indicated by the curly bracket.

(**C**) A pairing mechanism (dotted lines) occurs between the chimeric promoter's intron and the SD signal.

(**D**) Schematic representation of the contaminant vector; the sequence recognized by the SB probe is indicated with a blue curly bracket.

For this reason, we decided to substitute the chimeric intron with a new intron that is not homologous to the SD signal. We used a modified version of the SV40 intron [93], which was first cloned into a plasmid encoding for EGFP (Fig. 19A). HEK293T cells were then transfected with EGFP plasmids bearing either the chimeric intron or the SV40 intron to directly compare their ability to drive transgene expression. Fluorescence imaging (Fig. 19B) shows that EGFP expression from the construct containing the SV40 intron slightly outperforms the one from the chimeric intron, but overall has a similar efficacy.

A


B

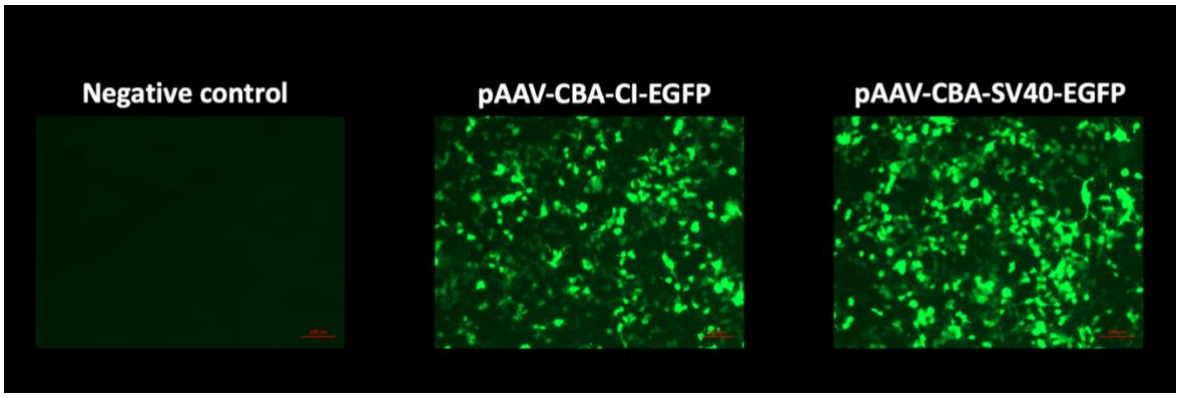


***Figure 19: In vitro comparison of the SV40 intron and the Chimeric intron by EGFP fluorescence***

**(A)** Representation of the plasmids encoding for EGFP with either the Chimeric intron (pAAV-CBA-CI-EGFP) or the SV40 intron (pAAV-CBA-SV40-EGFP).

**(B)** Representative microscope fluorescence pictures of transfected HEK293 cells (10X magnification, scale bar 100 μm). pAAV-CBA-CI-EGFP: plasmid encoding EGFP with Chimeric intron; pAAV-CBA-SV40-EGFP: plasmid encoding EGFP with SV40 intron.

After cloning the SV40 intron into the plasmid encoding 5'h*MYO7A* and producing the corresponding vector AAV-SV40-5'h*MYO7A* (Fig. 20A), we performed a second comparison against AAV-5'h*MYO7A* bearing the chimeric intron (AAV-CI-5'h*MYO7A*) by SB analysis of the purified viral DNA. We also subretinally injected C57BL/6 mice with either AAV-SV40-5'h*MYO7A* or AAV-CI-5'h*MYO7A* together with AAV-3'h*MYO7A*-3XFlag (dose 1.37E+10 total GC/eye) to evaluate hMYO7A expression levels by WB analysis. We found that the SV40 intron does not result in formation of the contaminant vector (Fig. 20B) and achieves similar hMYO7A expression levels *in vivo* (Fig. 20C-D). Therefore, we decided to use this version of AAV-5'h*MYO7A* to produce dual AAV-h*MYO7A* to be used in non-clinical and clinical studies.

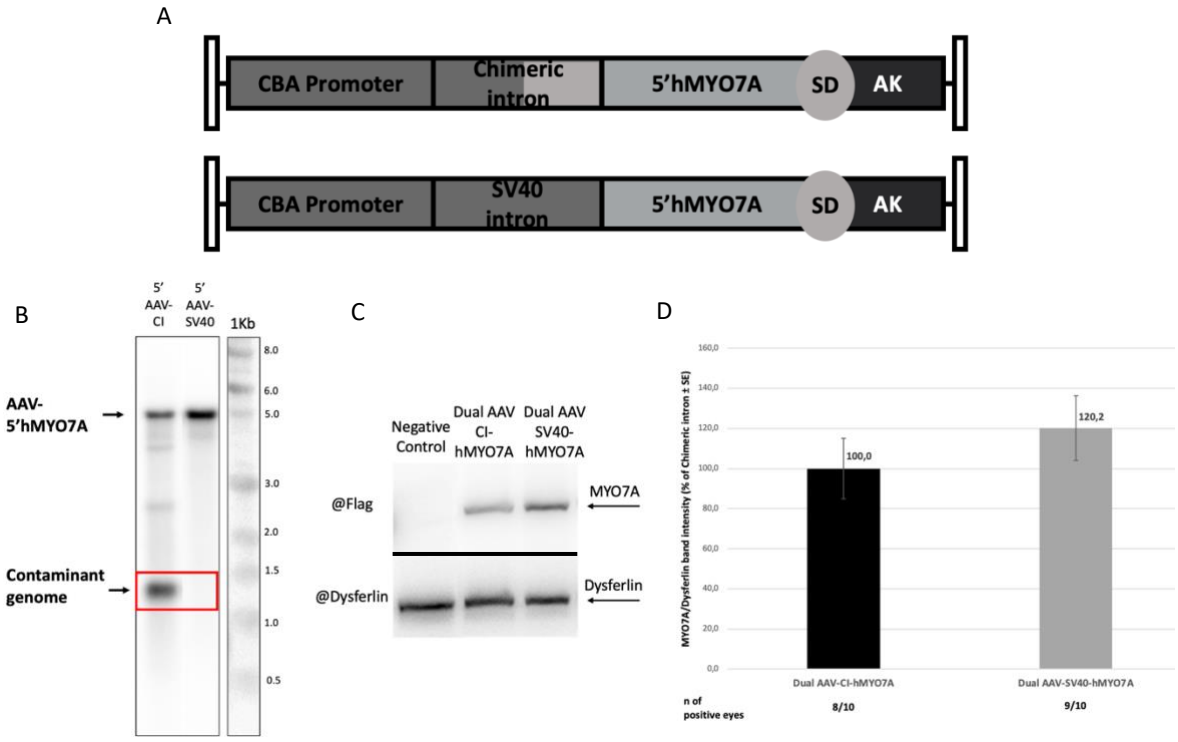


**For figure 20 caption see next page**

***Figure 20: In vivo comparison of the SV40 intron and the Chimeric intron***

**(A)** Schematic representation of the AAV-5'h*MYO7A* expression cassettes carrying either the chimeric intron (upper panel, AAV-CI-5'h*MYO7A*) or the SV40 intron (lower panel, AAV-SV40-5'h*MYO7A*).
**(B)** SB analysis performed on viral genomes extracted from either AAV-CI-5'h*MYO7A* or AAV-SV40-5'h*MYO7A*. The blue arrow indicates the correct genome, corresponding to AAV-5'h*MYO7A*, while the red arrow indicates the contaminant genome. The molecular weight marker is expressed in kilobases. Bp: base pair.
**(C)** Representative WB analysis of C57BL/6 eyecups 2 weeks following sub-retinal injection of either AAV-CI-5'h*MYO7A* or AAV-SV40-5'h*MYO7A* combined with AAV-3'h*MYO7A*-3XFlag (dual AAV-CI-h*MYO7A* and dual AAV-SV40-h*MYO7A*, respectively). As a negative control, eyes received a sub-retinal injection of the formulation buffer. The arrow indicates full-length proteins, 150 µg of proteins were loaded in each lane. @Flag: WB with anti-Flag antibody; @Dysferlin: Wb with anti-Dysferlin antibody, used as loading control.
**(D)** Quantification of hMYO7A protein levels in eyecups of C57BL/6 mice injected with either dual AAV-CI-hMYO7A or dual AAV-SV40-hMYO7A. hMYO7A band intensities was normalized to Dysferlin and levels were expressed as percentage of hMYO7A expressed in dual AAV-CI-h*MYO7A*-treated eyes. Data are represented as mean ± standard error of the mean (s.e.m.). The mean value is depicted above each bar. The number (n) of positive eyes for hMYO7A are depicted below each bar.

### *In vivo* safety of dual AAV-h*MYO7A* formulation buffer

AAV aggregation may have deleterious effects on vector transduction efficiency, biodistribution and immunogenicity and lead to a reduced yield during purification. It has been reported that AAV aggregation is reduced when the ionic strength of the formulation buffer is ≥ 200 mM [103]. The ionic strength of standard phosphate buffer saline (PBS) is 165 mM. To reach an ionic strength capable of preventing AAV aggregation, we decided to add 35 mM NaCl to the formulation buffer. First, we tested the osmolality of this formulation buffer, i.e. PBS/0.001% poloxamer 188 (P188)/NaCl 35 mM, in collaboration with our partners in Reithera, a good manufacturing practice (GMP) facility. The resulting osmolality was 364 mOsm which is in the osmolality range acceptable for human parenteral solution, i.e 300-400 mOsm. Then, we assessed the safety of this new formulation buffer (dual AAV excipient) *in vivo* by sub-retinal injection in C57BL/6 mice. To this end, we performed ERG to analyze the scotopic (log -4 to 1,3 cd.s/$m^2$) and photopic functional activity of the retina and SD-OCT to analyze retinal structure integrity. The modified formulation buffer was shown not to induce toxic effects compared to the control excipient, i.e. PBS/0.001% P188, 2 and 4 weeks post-injection (Fig. 21, two sample t-test statistical analysis. Panel A p-values: 0,0001 cd/$m^2$, A-wave = 0,519; B-wave = 0,468. 0,03 cd/$m^2$, A-wave = 0,815; B-wave = 0,720. 0,1 cd/$m^2$, A-wave = 0,519; B-wave = 0,474. 0,5

cd/$m^2$, A-wave = 0,967; B-wave = 0,765. 1 cd/$m^2$, A-wave = 0,361; B-wave = 0,671. 10 cd/$m^2$, A-wave = 0,893; B-wave = 0,767. 20 cd/$m^2$, A-wave = 0,804; B-wave = 0,298. Cones, A-wave = 0,575; B-wave = 0,689. Panel B p-values: 0,0001 cd/$m^2$, A-wave = 0,643; B-wave = 0,256. 0,03 cd/$m^2$, A-wave = 0,641; B-wave = 0,876. 0,1 cd/$m^2$, A-wave = 0,597; B-wave = 0,910. 0,5 cd/$m^2$, A-wave = 0,634; B-wave = 0,854. 1 cd/$m^2$, A-wave = 0,727; B-wave = 0,551. 10 cd/$m^2$, A-wave = 0,960; B-wave = 0,909. 20 cd/$m^2$, A-wave = 0,398; B-wave = 0,617. Cones, A-wave = 0,811; B-wave = 0,710. Fig.22, panel A, p-value at 16 days = 0,2868. Panel A, p-value at 5 weeks = 0,5742).

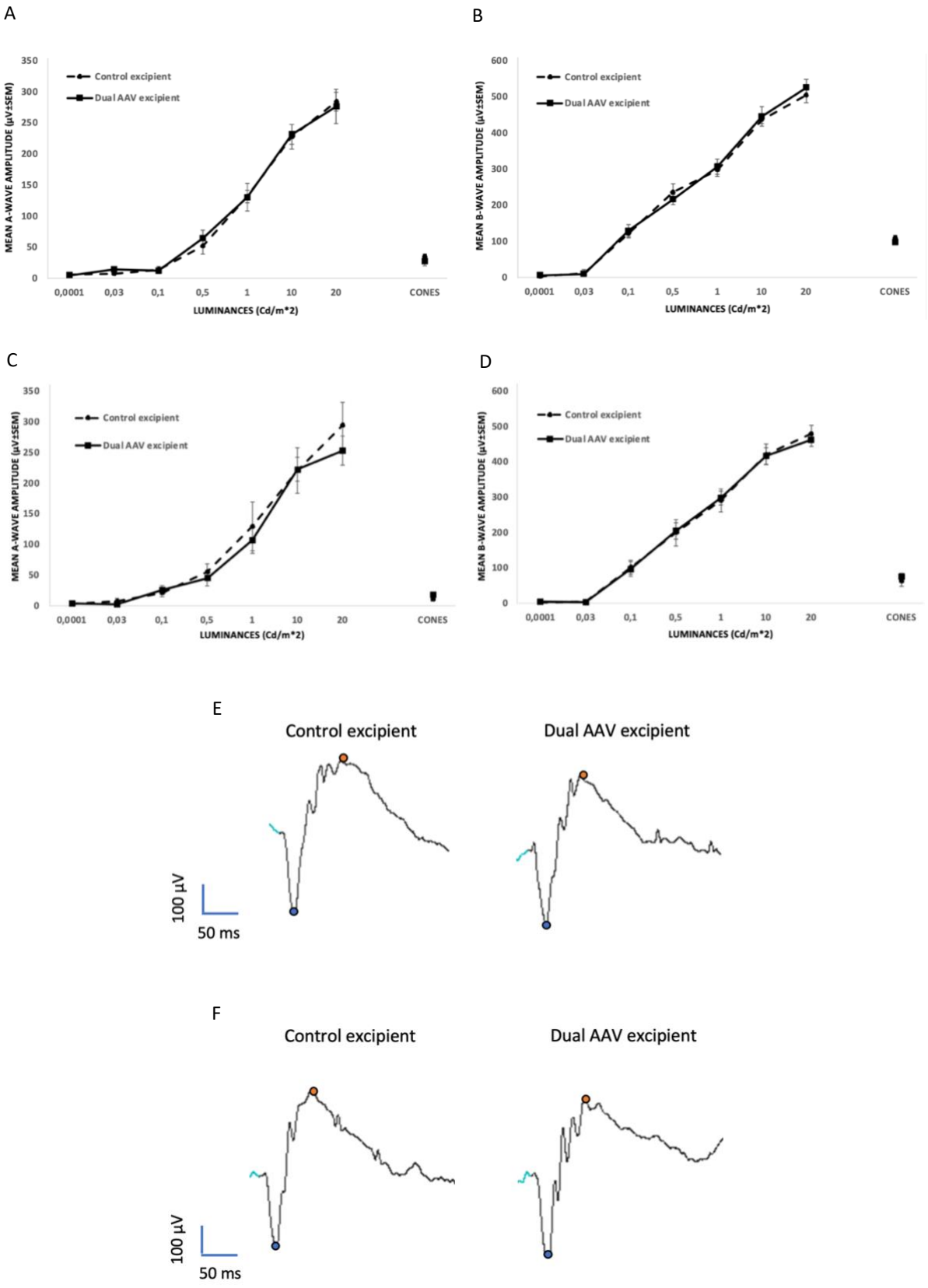


**For figure 21 caption see next page**

***Figure 21: Dual AAV-hMYO7A formulation buffer is safe following sub-retinal injection in C57BL/6 mice by electroretinogram analysis***

(**A**, **B**, **C**, **D**) Electroretinogram analysis performed on C57BL/6 mice 14 (**A**, **B**) and 28 (**C**, **D**) days after sub-retinal injection of either the dual AAV-h*MYO7A* formulation buffer or the control formulation buffer by measuring the A-wave (**A**, **C**) and the B-wave (**B**, **D**). Values are expressed in µV, luminances are indicated as cd/m$^2$. The number (n) of eyes for each group is 6. Values are represented as mean ± standard error of the mean (s.e.m.). Statistical analysis was conducted using two-sample t-test analysis.

**(E, F)** Representative ERG waves at 20 cd/m*2 of adult wild-type C57BL/6 mice 14 (**E**) or 28 (**F**) days after sub-retinal injection of either the dual AAV-h*MYO7A* formulation buffer or the control formulation buffer. Blue point indicates A-Wave, orange point indicates B-Wave. Vertical scale bar = 100 µV, horizontal scale bar = 50 ms. +/- : heterozygous unaffected *Oat* mice; -/- : homozygous affected *Oat* mice.

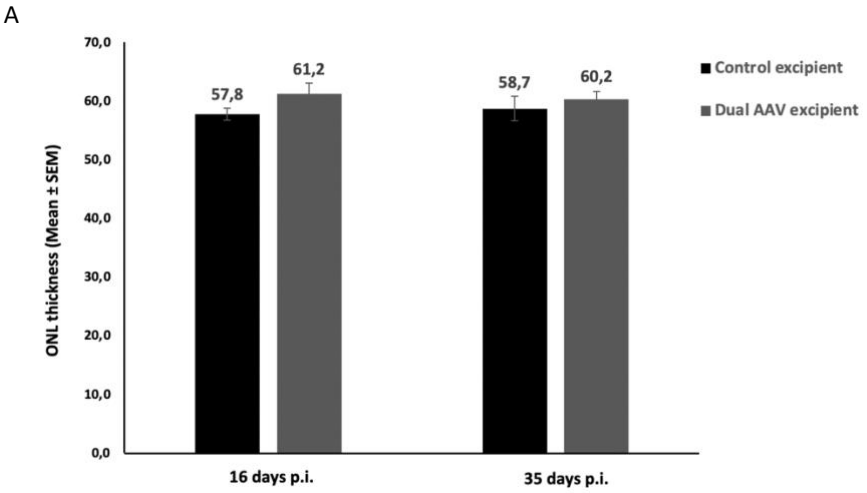


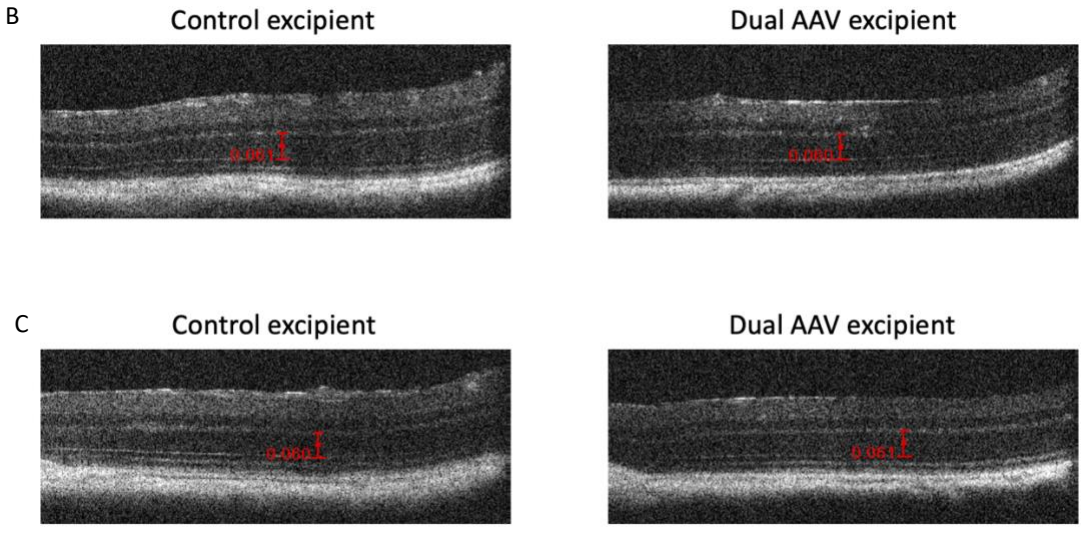


**For figure 22 caption see next page**

***Figure 22: Dual AAV-hMYO7A formulation buffer is safe following sub-retinal injection in C57BL/6 mice by spectral-domain optical coherence tomography analysis***

(**A**) The retinal outer nuclear layer (ONL) thickness was analysed by OCT in C57BL/6 mice 16 days and 35 days after sub-retinal injection of either the dual AAV-h*MYO7A* or the control formulation buffer. The number (n) of eyes for each group is 7. Values are represented as mean ± standard error of the mean (s.e.m.). The mean values are indicated above each bar, while time-points of analysis are indicated below each bar. Statistical analysis was conducted using two-sample t-test analysis.
(**B, C**) Representative retinal scannings of C57BL/6 mice 16 (**B**) and 35 (**C**) days after sub-retinal injection of either the dual AAV-h*MYO7A* or the control formulation buffer. Calipers for ONL measurements are in red and show mm of retinal thickness.

## Potency of dual AAV-h*MYO7A*

Two lots of dual AAV-h*MYO7A* were produced: a toxicology lot and a clinical lot. The toxicology lot (or tox lot) was produced, in collaboration with Reithera, using a manufacturing process representative of the GMP production process used to produce the clinical lot (GMP-lot). The tox lot was used to define the doses to be used in the clinical trial and to assess the safety of dual AAV-h*MYO7A* in non-clinical studies conducted under good laboratory practice. The clinical lot will be used to treat USH1B patients. Biological activity of these lots was tested in an *in vivo* transgene-related potency assay in subretinally injected shaker1$^{-/-}$ (sh1$^{-/-}$) mice. We plan to assess the stability, at the storage temperature < -60°C, of both lots yearly, up to 2 years for the tox lot and up to 5 years for the GMP-lot. WB analysis performed 5 weeks post-injection on whole eyecups confirmed the potency of both lots of dual AAV-h*MYO7A* up to the latest time-point of analysis.
Specifically, sh1$^{-/-}$ mice injected with the tox lot received a dose of 1.37E+10 total GC/eye which corresponds to 1X dose of the human clinical trial (1.37E+12 total GC/eye), considering that the human retinal surface is 100X larger than that of mice. At the first timepoint of evaluation, immediately after tox lot fill-in (timepoint 0), 4 out 8 eyes (50,0%) were positive for hMYO7A expression (fig. 23A). After one year of storage at < -60°C, all injected eyes (8 out 8, 100%) with dual AAV-h*MYO7A* had detectable hMYO7A expression (fig. 23B); this increase in number of positive eyes could be due to variability in rodents' sub-retinal injection, which is less controlled compared to sub-retinal injection in large mammals like humans.

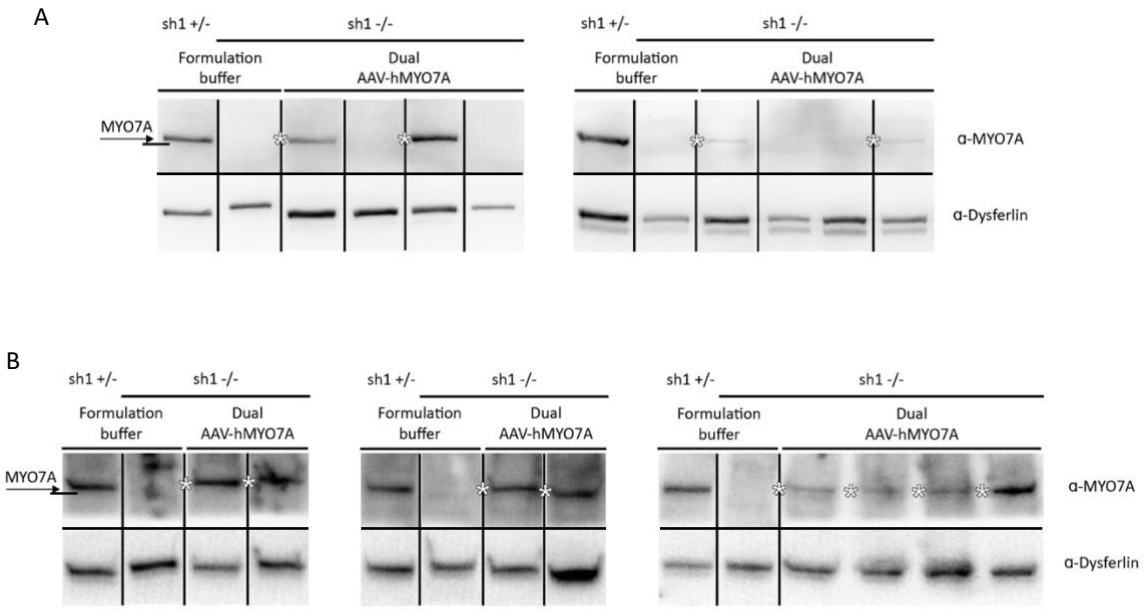


***Figure 23: In vivo transgene-related potency of dual AAV-hMYO7A tox lot***

WB analysis of hMYO7A was performed in eyecups from sh1 -/- mice that received a sub-retinal injection of either dual AAV-h*MYO7A* tox lot or formulation buffer. Analysis was performed at release (**A**) and after 1 year of storage at < -60°C (**B**). Sh1 -/- mice or normal heterozygous (sh1 +/-) mice received a sub-retinal injection of formulation buffer, as a negative or positive control, respectively. The arrow indicates full-length proteins, the bar depicted on the left indicates 250 kilodalton, 150 µg of proteins were loaded in each lane. White asterisks indicate eyes positive for hMYO7A expression. α-MYO7A: WB with anti-MYO7A antibody; α-Dysferlin: WB with anti-Dysferlin antibody, used as loading control.

The GMP-lot was injected at a lower dose than the tox lot, due to a lower vector titer and restrictions to the injection volume that can be administered subretinally in mice; specifically, a dose of 4,6E+9 total GC/eye (∽3X lower than the one used to test the *in vivo* potency of the tox lot) was delivered subretinally to sh1$^{-/-}$ mice. Nevertheless, at the release of GMP-lot, 5 out of 8 eyes were positive for hMYO7A expression (62,5%) (fig.24A) while after one year of storage at < -60°C, 6 out of 8 eyes were positive (75,0%) (fig.24B).

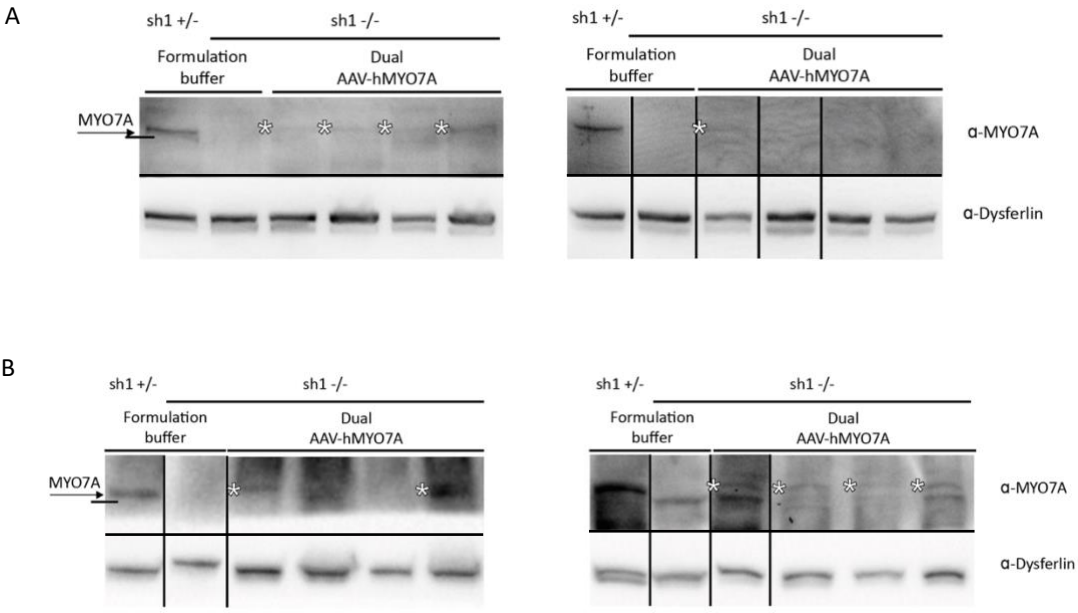


***Figure 24: In vivo transgene-related potency of dual AAV-hMYO7A GMP-lot***

WB analysis of hMYO7A was performed in eyecups from sh1 -/- mice that received a sub-retinal injection of either dual AAV-h*MYO7A* GMP-lot or formulation buffer. Analysis was performed at release (**A**) and after 1 year of storage at < -60°C (**B**). Sh1 -/- mice or normal heterozygous (sh1 +/-) mice received a sub-retinal injection of formulation buffer, as a negative and positive control, respectively. The arrow indicates full-length proteins, the bar depicted on the left indicates 250 kilodalton, 150 µg of proteins were loaded in each lane. White asterisks indicate eyes positive for hMYO7A expression. α-MYO7A: WB with anti-MYO7A antibody; α-Dysferlin: WB with anti-Dysferlin antibody, used as loading control.

## Dual AAV-h*MYO7A* dose response study

To select doses to be used in USH1B subjects, we performed a dose response study using the dual AAV-h*MYO7A* tox lot. Subretinally injected sh1$^{-/-}$ mice were analyzed for rescue of retinal defects and protein hMYO7A levels. We selected three different doses: 1,37E+9 (low dose or LD), 4,4E+9 (medium dose or MD), and 1,37E+10 (high dose or HD) total GC/eye. Unaffected heterozygous mice and affected mice injected with the formulation buffer only were used as positive and negative controls, respectively. Sh1$^{-/-}$ mice display ultrastructural defects of the retina, as almost no melanosomes are located to the RPE apical villi. Three months post-injection, we confirmed the dose-dependent effects by measuring the number of correctly localized melanosomes to the RPE apical villi (Fig. 25A-B). Injection of HD and MD of dual AAV-h*MYO7A* significantly rescued retinal defects compared to sh1$^{-/-}$ that only received formulation buffer; moreover, there was no statistical difference between unaffected eyes and affected eyes treated with HD (fig. 25A, pANOVA values:

affected sh1$^{-/-}$ injected with formulation buffer vs either unaffected sh1$^{+/-}$ injected with formulation buffer < 0,0001, sh1$^{-/-}$ treated with the high dose < 0,0001, sh1$^{-/-}$ treated with the medium dose <0,01 or sh1$^{-/-}$ treated with the low dose = 0,313; sh1$^{-/-}$ treated with the high dose vs either unaffected sh1$^{+/-}$ injected with formulation buffer = 0,105, sh1$^{-/-}$ treated with the medium dose = 0,113 or sh1-/- treated with the low dose < 0,01; sh1$^{-/-}$ treated with the medium dose vs either unaffected sh1$^{+/-}$ injected with formulation buffer < 0,001 or sh1$^{-/-}$ treated with the low dose = 0,442; unaffected sh1$^{+/-}$ injected with formulation buffer vs sh1$^{-/-}$ treated with the low dose < 0,0001). Sh1$^{-/-}$ LD-treated eyes also showed correction of the retinal phenotype compared to the negative control, although with no statistical significance in the whole retinal section. This was due to variability within the unaffected sh1$^{+/-}$ group that affected statistical analysis, thus we repeated the ANOVA analysis without unaffected sh1$^{+/-}$ and reached statistical significance for the LD as well (pANOVA values: affected sh1$^{-/-}$ injected with formulation buffer vs sh1-/- treated with the high dose < 0,0001, sh1$^{-/-}$ treated with the medium dose <0,0001 or sh1$^{-/-}$ treated with the low dose < 0,01; sh1$^{-/-}$ treated with the high dose vs either sh1$^{-/-}$ treated with the medium dose < 0,001 or sh1$^{-/-}$ treated with the low dose < 0,0001; sh1$^{-/-}$ treated with the medium dose vs sh1$^{-/-}$ treated with the low dose < 0,05).

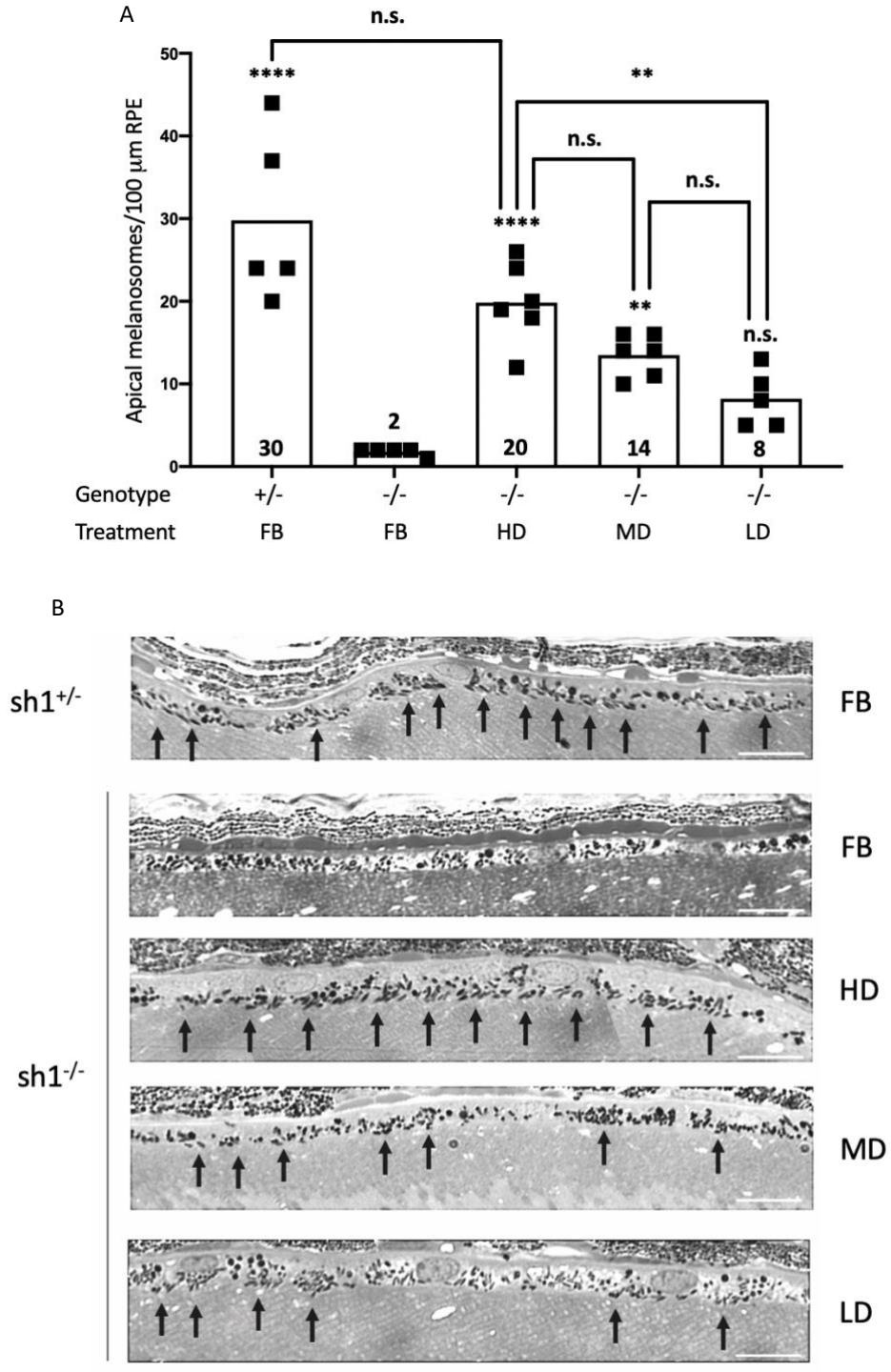


**For figure 25 caption see next page**

***Figure 25: Sub-retinal administration of dual AAV-hMYO7A results in dose-dependent improvements to retinal defects in sh1$^{-/-}$ mice***

**(A)** Quantification of correctly localized melanosomes was performed in sh1$^{-/-}$ mice receiving dual AAV-h*MYO7A* at low dose (LD, 1.37E+9 total GC/eye), medium dose (MD, 4.4E+9 total GC/eye), high dose (HD, 1.37E+10 total GC/eye), or formulation buffer only, as a control condition. As an unaffected control, sh1$^{+/-}$ mice were injected with formulation buffer only. For each eye, the number of apical melanosomes per 100 µm of Retinal Pigment Epithelium (RPE) was measured. Results are represented as mean value for each eye (filled square) and as mean value for each treatment group (reported inside or above each column). Statistical analysis was performed using one-way ANOVA followed by the Tukey post-hoc test. Stars above each column refer to the comparison against sh1$^{-/-}$ receiving formulation buffer (FB): * p<0,05; ** p<0,01; **** p <0,0001. n.s.: no significant difference.

**(B)** Representative pictures from montages of the entire retinal section imaged at 100X magnification and used for melanosomes analysis. Each picture is composed of ∽3 fields. Scale bar (white bar) = 10 µm. Black arrows point at correctly localized melanosomes. FB: formulation buffer; HD: high dose; MD: medium dose; LD: low dose.

WB analysis of lysed eyecups (RPE + neural retina) from sh1$^{-/-}$ mice 5 weeks after sub-retinal injection displays expression of the full length hMYO7A for all selected doses of dual AAV-h*MYO7A* (Fig. 26A). A higher number of eyes were positive for hMYO7A expression using the HD and the MD compared to the LD (Fig. 26B).

A

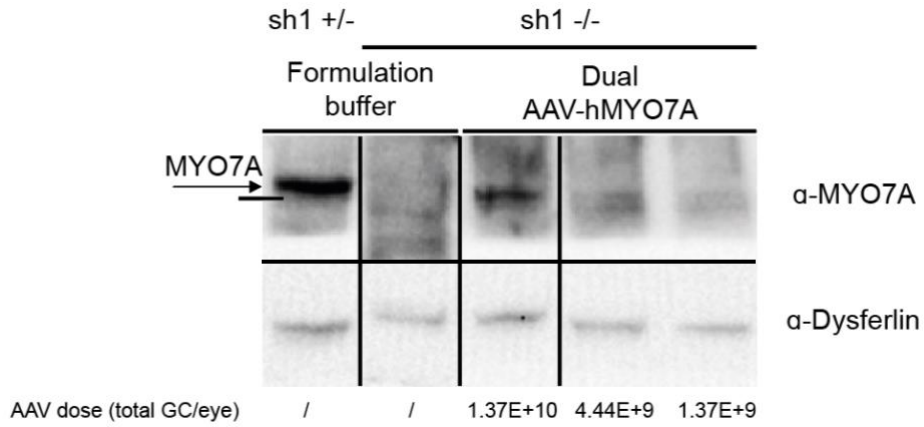


B

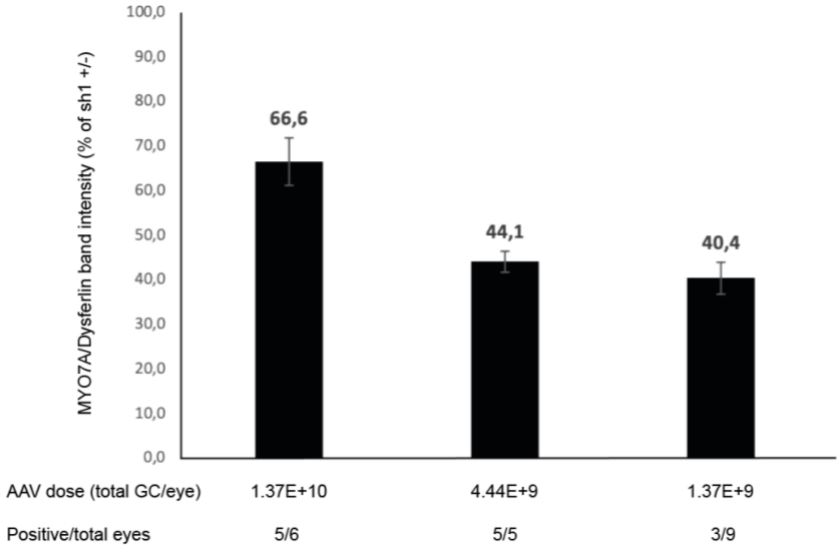


**For figure 26 caption see next page**

***Figure 26: Dose-dependent effects of dual AAV-hMYO7A on hMYO7A expression in sh1$^{-/-}$ mice***

**(A)** Representative WB analysis of sh1 eyecups 5 weeks following sub-retinal injection of either dual AAV-h*MYO7A* or formulation buffer. The arrow indicates full-length proteins, the bar depicted on the left indicates 250 kilodalton, 150 µg of proteins were loaded in each lane. HD: dual AAV-h*MYO7A* high dose (1.37E+10 total GC/eye); MD: dual AAV-h*MYO7A* medium dose (4.4E+9 total GC/eye); LD: dual AAV-h*MYO7A* low dose (1.37E+9 total GC/eye); α-MYO7A: WB with anti-MYO7A antibody; α-Dysferlin: WB with anti-Dysferlin antibody, used as loading control.

**(B)** Quantification of hMYO7A protein levels in eyecups of sh1$^{-/-}$ mice subretinally injected with dual AAV-h*MYO7A* relative to endogenous Myo7a expressed in littermate sh1$^{+/-}$ eyecups. hMYO7A and Myo7a band intensities were normalized to Dysferlin and the data are reported as percentage (%) relative to sh1+/-Myo7a. Values are represented as mean ± standard error of the mean (s.e.m.); the mean value is reported above each bar. Number of hMYO7A positive eyes/total eyes for each treatment are reported below each bar.

## DISCUSSION

AAV-mediated gene therapy of the retina has reached maturity. The success of Luxturna to treat Leber Congenital Amaurosis type 2 has expanded AAV applicability to treat other inherited retinal diseases (IRDs) [74], [75], [78]. AAV vectors are non-integrating, non-pathogenic, and are able to diffuse and transduce all retinal layers upon a single sub-retinal injection across several species [65]–[69]. Non-integrating vectors are most suitable for use in non-dividing cells such as photoreceptors, which are the main target for gene therapy of the eye. Finally, the small enclosed environment of the eye enhances co-infection of two or more vectors each carrying a portion of a long coding sequence, solving one of the few limitations of AAV vectors, the DNA cargo capacity [86], [104].

We focused our attention on two rare IRDs, gyrate atrophy of the choroid and retina (GA) and Usher syndrome type 1B (USH1B) retinitis pigmentosa. Although relatively few patients are affected by these diseases (GA = 1:50000 in Finland [7]; USH1B: 1:30000-42000 worldwide [28]), their collective social and economic impacts are tremendous. Blind and blind-deaf people are harder to integrate in the modern society due to difficulties in communicating and living independently. This has national economic implications as health systems consequently need to provide palliative treatments and 24h-support assistance. Since no curative treatments are currently available for inherited blindness, gene therapy of the retina represents an efficient, cost-effective approach to save or restore eyesight in patients.

GA is a rare inborn error of metabolism characterized by the absence of *ornithine aminotransferase* (*OAT*), hyperornithinemia and degeneration of retinal pigment epithelial (RPE) cells leading to blindness [7], [9], [15]. OAT is an enzyme working at the intersection between the urea cycle and aminoacid biosynthesis [11]. Many studies on GA revolve around a mouse model missing the third exon of the target gene Oat ($Oat^{-/-}$) causing hyperornithinemia and RPE degeneration [13], [20], [105]. Importantly, an arginine-restricted diet in this mouse model lowered ornithine systemic levels and improved retinal electrical responses and retinal morphology [105]. However, a similar strict dietary regime in clinics showed limited efficacy in adult patients and only few young patients were able to successfully follow this diet [22]. Gene therapy of GA with AAV could induce long-term expression of OAT with just a single administration. In aim 1, I designed an expression cassette for the human *OAT* (h*OAT*) enzyme with a 3XFlag tag and demonstrated correct expression and enzymatic activity in two different cell lines with relative low expression of

OAT. Then, we produced an AAV encoding for h*OAT*-3XFlag (AAV-h*OAT*-3XFlag) and subretinally injected adult wild type mice [dose 3,0E+9 genome copies (GC)/eye]. Western blot (WB) analysis confirmed expression of h*OAT*-3XFlag in 100% of the injected eyes. OAT activity was not significantly different in wild type eyecups injected with AAV-h*OAT*-3XFlag compared to contralateral eyes injected with vehicle, and the AAV-injected eyes show a slight lower activity on average. We hypothesize that this is due to heterodimerization between hOAT monomers and murine Oat (mOat) with lower activity. Sub-retinal injection of AAV-h*OAT*-3XFlag (dose 5,4E+9 GC/eye) in $Oat^{-/-}$ mice improved the outer nuclear layer thickness retinal structure, as shown by OCT at an early timepoint of the disease (4 months of age). At the same timepoint, no functional differences in retinal electrical activity were detected by ERG analysis of the A-wave and B-wave in eyes receiving AAV-h*OAT*-3XFlag compared to contralateral eyes injected with formulation buffer. As a future plan, retinal morphology and electrical activity will be assessed with a longer timeframe to evaluate beneficial effects of AAV-h*OAT*-3XFlag treatment on both retinal structure and function. Additionally, we plan to perform the OAT activity assay and retinal histology analysis to confirm that hOAT expression is successfully rescuing RPE and retinal cells in $Oat^{-/-}$ eyes subretinally injected with AAV-h*OAT*-3XFlag.

In aim 2, I produced data required for the clinical translation of a gene therapy approach based on dual AAV vectors encoding human *Myosin7A* (dual AAV-h*MYO7A*) to treat USH1B retinitis pigmentosa. USH1B is characterized by congenital deafness and blindness due to biallelic mutations in the large motor protein Myosin7A (MYO7A); although hearing impairment can be counteracted with a cochlear implant, currently no treatment is available for blindness due to retinitis pigmentosa in USH1B patients [29]. Gene therapy with AAV is a valid option for treatment, however the *Myosin7A* (*MYO7A*) coding sequence does not fit in a single AAV (cargo capacity < 5 Kb). To solve this issue, we demonstrated that gene therapy with two AAVs induces therapeutic expression of human *MYO7A* (dual AAV-h*MYO7A*) exploiting inverted-terminal repeat (ITR)-mediated concatemerization. Sub-retinal injection of dual AAV-h*MYO7A* in the $shaker1^{-/-}$ ($sh1^{-/-}$) mouse model of USH1B improved number of correctly localized melanosomes to the RPE apical villi, which is impaired in USH1B [86], [90]. As we moved towards the clinical translation of this approach, we discovered the presence of two different viral genomes in the AAV preparation encoding for the 5' of h*MYO7A* (AAV-5'h*MYO7A*) by a southern blot using a probe designed designed to recognize the promoter sequence. One genome corresponds to AAV-5'h*MYO7A* while the other is a much smaller contaminant that could be packaged once,

twice or even three times in the same AAV particle. Careful analysis of the expression cassette showed perfect similarity between the splicing donor site of dual AAV and the 5' portion of the chimeric promoter's intron. This similarity (82 bp) leads to a recombination event that cause deletion of the remaining portion of the intron, the 5'-h*MYO7A* sequence and the splicing donor sequence, thus leaving the ITRs intact. To overcome this issue, I selected a promoter intron, with no similarity to the splicing donor, which maintains hMYO7A expression at levels comparable to the chimeric intron while avoiding the formation of the contaminant genome.

AAV adhesion to the surgical device and viral particle aggregation are known issues that may change the fate of a clinical trial. To this end, we used a formulation buffer for dual AAV-h*MYO7A* composed of commercial phosphate buffer saline (PBS) supplemented with poloxamer 188 (P188), an FDA-approved drug that prevents AAV adhesion and was recently used in a clinical trial for choroideremia [106], [107]. Moreover, it has been reported that AAV aggregation can be reduced when the ionic strength of the formulation buffer is ≥ 200 mM [103]. For our formulation buffer, we added 35 mM NaCl to reach this ionic strength, while maintaining the osmolality within the acceptable range for human parenteral solution (200-300 mOsm). Afterwards, we tested the formulation buffer safety in adult C57BL/6 mice by sub-retinal injection; compared to the control formulation buffer (PBS+P188), our custom formulation buffer did not alter retinal electrical activity (both scotopic and photopic) and retinal outer nuclear layer thickness at 2 and 4 weeks post-injection.

In collaboration with Reithera, a good manufacturing practice (GMP) facility and partners for the clinical translation of dual AAV-h*MYO7A*, we produced two GMP lots of dual AAV-h*MYO7A*: a toxicology lot (tox lot) for pre-clinical studies and a clinical lot that will be used to treat retinitis pigmentosa in USH1B patients. We designed an *in vivo* transgene-related potency assay by WB analysis of sh1$^{-/-}$ eyecups to assess the number of eyes expressing hMYO7A and confirm efficacy and long-term stability at the storage temperature (<-60°C) of both lots of dual AAV-h*MYO7A*. Results confirmed the stability of both the tox lot and the clinical lot up to 1-year post-production. Our plan is to address stability of the clinical lot yearly up to 5 years of storage at <-60°C to support the use of the medicinal product in USH1B patients.

The tox lot was used 1) to select doses to be used in the clinical trial and 2) in non-clinical studies conducted under good laboratory practice (GLP) to assess the safety of dual AAV-h*MYO7A*. As required for first-in-humans studies, we performed a dose-response study of

dual AAV-h*MYO7A* in subretinally injected sh1$^{-/-}$ to select doses to be used in USH1B patients. From our previously reported works and other AAV clinical trials [72]–[76], [86], [90], we tested 3 doses of dual AAV-h*MYO7A*, ranging from 1,37E+9 (LD) – 4,44E+9 (MD) – 1,37E+10 (HD) total GC/eye, for correction of RPE melanosomes and hMYO7A expression. All selected doses induce hMYO7A expression as shown by WB analysis of total eyecups. The number of apical melanosomes in sh1$^{-/-}$ administered with either HD or MD doses was significantly improved in comparison to control sh1$^{-/-}$ mice injected with the vehicle (formulation buffer). Importantly, sh1$^{-/-}$ eyes receiving the HD were not significantly different to the unaffected eyes, sh1$^{+/-}$ eyes injected with the vehicle. An increased number of apical melanosomes, albeit not statistically significant, was also observed in sh1$^{-/-}$ mice administered with the LD, suggesting that the dose of 1,37E+9 total GC/eye of dual AAV-h*MYO7A* could be considered as the minimal effective dose. Finally, as the human retinal surface is about 100-fold larger than the murine one, we can infer that therapeutics doses in USH1B subjects should range between 1,37E+11 and 1,37E+12 total GC/eye of dual AAV-h*MYO7A*.

In view of clinical translation, the safety of dual AAV-h*MYO7A* will be assessed in a GLP study conducted in non-human primates (NHPs), a relevant animal model for evaluation of ocular therapy. The human and the macaque eye share the highest similarities, thus allowing the correct safety studies to be performed: 1) only primate retinas are characterized by the macula, a structure with the highest concentration of cones photoreceptors compared to the rest of the retina and required for central vision; 2) the dimensions of the macaque eye is similar to that of humans; 3) the sub-retinal injection with an anterior trans-scleral approach followed by partial vitrectomy can be performed in both human and macaque eyes; 4) the same injection volume, two blebs of 150 µL each, can be used in both species. A 13-weeks study was designed using two different doses of GMP-like dual AAV-h*MYO7A* to test the safety, route of delivery, biodistribution, expression and immune responses of dual AAV-h*MYO7A*. The study comprises three groups receiving a single sub-retinal injection in the right eye of: vector excipient (control group), 1,37E+12 total GC/eye (low dose group), and 3,75E+12 total GC/eye (high dose group) of dual AAV-h*MYO7A*. Systemic safety in subretinally injected NHPs will be confirmed by evaluation of general health markers (body weight, electrocardiogram, blood tests, urianalysis) and histopathology. Ocular safety will be assessed by *in vivo* evaluations, such as ERG analysis, fundoscopy, fluorangiography and optical coherence tomography, and *ex vivo* by histopathology. The success of this project could pave the way for the application

of AAVs to a larger number of diseases due to mutations in coding sequences larger than the AAV cargo capacity.

## CONCLUSIONS

During my Ph.D. thesis, I developed adeno-associated viral (AAV) vectors to deliver small and large expression cassettes to the eye and produce pre-clinically relevant data in animal models of two inherited retinal diseases (IRDs), gyrate atrophy of the choroid and retina (GA) and Usher syndrome type 1B (USH1B) retinitis pigmentosa.

Absence of the *ornithine aminotransferase* (*OAT*) enzyme leads to GA and to selective toxicity for retinal pigment epithelial (RPE) cells. Upon transfection of a plasmid encoding for human *OAT* (h*OAT*), I demonstrated expression of this enzyme *in vitro* in two cell lines, HeLa and hARPE-19 cells, and increased OAT enzymatic activity. Upon sub-retinal injection of an AAV encoding for h*OAT* (AAV-h*OAT*) in adult C57BL/6 mice, we were able to detect human *ornithine aminotransferase* (h*OAT*) expression in all injected eyecups. AAV-h*OAT* sub-retinal treatment in an *Oat*$^{-/-}$ mouse model of GA improved retinal morphology at an early time-point of the disease.

Usher syndrome type 1B (USH1B), a disease characterized by retinitis pigmentosa (RP), is caused by lack of the large motor protein Myosin7A (MYO7A), which does not fit into a single AAV vector [29]. Our group was able to induce therapeutical expression of the full length human *Myosin*7A (h*MYO7A*) using two AAVs (dual AAV-h*MYO7A*) and exploiting ITR-mediated concatemerization [86], [90]. After detecting an unexpected contaminant vector, which could impact the efficiency of the dual AAV-h*MYO7A* approach, we identified causative sequence similarity in the expression cassette. I was able to successfully change one of the sequences to avoid production of the contaminant while achieving similar expression levels of the full length human *MYO7A* (h*MYO7A*) *in vivo*. We performed clinical translation of dual AAV vectors for USH1B retinitis pigmentosa (UshTher project – grant n. 754848) after evaluating the safety and potency of dual AAV-h*MYO7A*. We assessed the potency of dual AAV-h*MYO7A*, produced under good manufacturing practices (GMP), in an *in vivo* transgene-related assay, confirming biological activity of dual AAV-h*MYO7A* in subretinally injected shaker1$^{-/-}$ (sh1$^{-/-}$) mice. This assay will be used yearly, up to 5 years, to confirm stability of the GMP lot that will be used in USH1B patients. Finally, as this project was considered first use of dual AAV vectors in the human eye, we selected three doses of dual AAV-h*MYO7A* (1.37E+9 – 4.44E+9 – 1.37E+10 total genome copies (GC)/eye) and confirmed dose-dependent effects by assessing the number of correctly localized melanosomes; results indicate that larger portions of the retina benefit from increasing the dose of dual AAV-h*MYO7A*.

Overall, the results of these studies support the clinical translation of single and dual AAV vectors for gene therapy of GA and USH1B retinitis pigmentosa.

## REFERENCES


[1] S. Kawamura and S. Tachibanaki, “Explaining the functional differences of rods versus cones,” *Wiley Interdiscip. Rev. Membr. Transp. Signal.*, vol. 1, no. 5, pp. 675–683, 2012, doi: 10.1002/wmts.8.

[2] O. Strauss, “The retinal pigment epithelium in visual function,” *Physiol. Rev.*, vol. 85, no. 3, pp. 845–881, 2005, doi: 10.1152/physrev.00021.2004.

[3] I. J. M. S Beatty, M Boulton, D Henson, H-H Koh, “Macular pigment and age-related macular degeneration,” *J.Ophtalmology*, vol. 64, no. 4, pp. 409–415, 2010.

[4] A. W. Scott, N. M. Bressler, S. Ffolkes, J. S. Wittenborn, and J. Jorkasky, “Public attitudes about eye and vision health,” *JAMA Ophthalmol.*, vol. 134, no. 10, pp. 1111–1118, 2016, doi: 10.1001/jamaophthalmol.2016.2627.

[5] W. Berger, B. Kloeckener-Gruissem, and J. Neidhardt, “The molecular basis of human retinal and vitreoretinal diseases,” *Prog. Retin. Eye Res.*, vol. 29, no. 5, pp. 335–375, 2010, doi: 10.1016/j.preteyeres.2010.03.004.

[6] J. E., “Ein Fall von Retinitis Pigmentosa atypica.,” *Klin Monatsbl Augenheilkd*, vol. 26:202–6, 1888.

[7] K. K. Takki and R. C. Milton, “The Natural History of Gyrate Atrophy of the Choroid and Retina,” *Ophthalmology*, vol. 88, no. 4, pp. 292–301, 1981, doi: 10.1016/S0161-6420(81)35031-3.

[8] D. V. M.Kaiser-Kupfer, R.Caruso, “Gyrate atrophy of the choroid and retina: Further Experience With Long-term Reduction of Ornithine Levels in Children,” *Postgrad. Med. J.*, vol. 120, 2002, doi: 10.1136/postgradmedj-2021-139807.

[9] K. E. Peltola *et al.*, “Ophthalmologic heterogeneity in subjects with gyrate atrophy of choroid and retina harboring the L402P mutation of ornithine aminotransferase,” *Ophthalmology*, vol. 108, no. 4, pp. 721–729, 2001, doi: 10.1016/S0161-6420(00)00587-X.

[10] R. Montioli, I. Bellezza, M. A. Desbats, C. Borri Voltattorni, L. Salviati, and B. Cellini, “Deficit of human ornithine aminotransferase in gyrate atrophy: Molecular, cellular, and clinical aspects,” *Biochim. Biophys. Acta - Proteins Proteomics*, vol. 1869, no. 1, p. 140555, 2021, doi: 10.1016/j.bbapap.2020.140555.

[11] B. W. Shen, M. Hennig, E. Hohenester, J. N. Jansonius, and T. Schirmer, “Crystal structure of human recombinant ornithine aminotransferase,” *J. Mol. Biol.*, vol.

277, no. 1, pp. 81–102, 1998, doi: 10.1006/jmbi.1997.1583.

[12] K. Ratzlaff and A. Baich, “Comparison of ornithine aminotransferase activities in the pigment epithelium and retina of vertebrates,” *Comp. Biochem. Physiol. -- Part B Biochem.*, vol. 88, no. 1, pp. 35–37, 1987, doi: 10.1016/0305-0491(87)90075-7.

[13] T. Wang, A. H. Milam, G. Steel, and D. Valle, “A mouse model of gyrate atrophy of the choroid and retina: Early retinal pigment epithelium damage and progressive retinal degeneration,” *J. Clin. Invest.*, vol. 97, no. 12, pp. 2753–2762, 1996, doi: 10.1172/JCI118730.

[14] S. L. Bernstein and P. Wong, “Regional expression of disease-related genes in human and monkey retina.,” *Mol. Vis.*, vol. 4, no. May, p. 24, 1998, doi: 10.7939/R3N29P68P.

[15] M. I. Kaiser-Kupfer *et al.*, “Systemic Manifestations of Gyrate Atrophy of the Choroid and Retina,” *Ophthalmology*, vol. 88, no. 4, pp. 302–306, 1981, doi: 10.1016/S0161-6420(81)35030-1.

[16] K. Heinänen *et al.*, “Muscle creatine phosphate in gyrate atrophy of the choroid and retina with hyperornithinaemia - Clues to pathogenesis,” *Eur. J. Clin. Invest.*, vol. 29, no. 5, pp. 426–431, 1999, doi: 10.1046/j.1365-2362.1999.00467.x.

[17] M. Valtonen *et al.*, “Central nervous system involvement in gyrate atrophy of the choroid and retina with hyperornithinaemia,” *J. Inherit. Metab. Dis.*, vol. 22, no. 8, pp. 855–866, 1999, doi: 10.1023/A:1005602405349.

[18] R. Santinelli *et al.*, “Low-protein diet and progression of retinal degeneration in gyrate atrophy of the choroid and retina: A twenty-six-year follow-up,” *J. Inherit. Metab. Dis.*, vol. 27, no. 2, pp. 187–196, 2004, doi: 10.1023/B:BOLI.0000028779.29966.05.

[19] M. A. Cleary *et al.*, “Ornithine aminotransferase deficiency: Diagnostic difficulties in neonatal presentation,” *J. Inherit. Metab. Dis.*, vol. 28, no. 5, pp. 673–679, 2005, doi: 10.1007/s10545-005-0074-1.

[20] D. V. T.Wang, A.M. Lawler, G.Steel, I.Sipila, A.H. Milam, “Mice lacking ornithine-delta-aminotransferase have paradoxical neonatal hypoornithinaemia and retinal degeneration,” *Nature*, vol. 2, no. 11, pp. 983–989, 1995.

[21] K. M. Palanza, A. V. Nesta, R. Tumu, C. M. Walton, M. A. Davis, and T. R. King, “Auxotrophy-based detection of hyperornithinemia in mouse blood and urine,” *J. Inborn Errors Metab. Screen.*, vol. 4, pp. 1–8, 2016, doi: 10.1177/2326409816649600.

[22] I. S. K.Vannas-Sulonen, O.Simell, “Gyrate Atrophy of Choroid and Retina: The Ocular Disease Progresses in juvenile Patients despite Normal or Near Normal Plasma Ornithine Concentration,” *J. Indian Med. Assoc.*, vol. 100, no. 3, pp. 196–197, 2002, doi: 10.1016/s0161-6420(87)33269-5.

[23] M. Vernon, “Sociological and psychological factors associated with hearing loss.,” *J. Speech Hear. Res.*, vol. 12, no. 3, pp. 541–563, 1969, doi: 10.1044/jshr.1203.541.

[24] H. M. Fortnum, A. Q. Summerfield, D. H. Marshall, A. C. Davis, and J. M. Bamford, “Prevalence of permanent childhood hearing impairment in the United Kingdom and implications for universal neonatal hearing screening: Questionnaire based ascertainment study,” *Br. Med. J.*, vol. 323, no. 7312, pp. 536–539, 2001.

[25] J. A. Boughman, M. Vernon, and K. A. Shaver, “Usher syndrome: Definition and estimate of prevalence from two high-risk populations,” *J. Chronic Dis.*, vol. 36, no. 8, pp. 595–603, 1983, doi: 10.1016/0021-9681(83)90147-9.

[26] M. L. Marazita, L. M. Ploughman, B. Rawlings, E. Remington, K. S. Arnos, and W. E. Nance, “Genetic epidemiological studies of early-onset deafness in the U.S. school-age population,” *Am. J. Med. Genet.*, vol. 46, no. 5, pp. 486–491, 1993, doi: 10.1002/ajmg.1320460504.

[27] C. R. Otterstedde, U. Spandau, A. Blankenagel, W. J. Kimberling, and C. Reisser, “A new clinical classification for Usher’s syndrome based on a new subtype of Usher’s syndrome type I,” *Laryngoscope*, vol. 111, no. 1, pp. 84–86, 2001, doi: 10.1097/00005537-200101000-00014.

[28] R. G. Gregory-Evans, K., Pennesi, M.E., and Weleber, “Retinitis Pigmentosa and Allied Disorders,” *In Retina, S.J. Ryan, ed. (Elsevier)*, 2013. .

[29] J. M. Millán, E. Aller, T. Jaijo, F. Blanco-Kelly, A. Gimenez-Pardo, and C. Ayuso, “An Update on the Genetics of Usher Syndrome,” *J. Ophthalmol.*, vol. 2011, pp. 1–8, 2011, doi: 10.1155/2011/417217.

[30] X. Liu, G. Vansant, I. P. Udovichenko, U. Wolfrum, and D. S. Williams, “Myosin VIIa, the product of the Usher 1B syndrome gene, is concentrated in the connecting cilia of photoreceptor cells,” *Cell Motil. Cytoskeleton*, vol. 37, no. 3, pp. 240–252, 1997, doi: 10.1002/(SICI)1097-0169(1997)37:3<240::AID-CM6>3.0.CO;2-A.

[31] X. Liu, B. Ondek, and D. S. Williams, “Mutant myosin VIIa causes defective melanosome distribution in the RPE of shaker-1 mice.,” *Nat. Genet.*, vol. 19, no. 2, pp. 117–118, 1998, doi: 10.1038/470.

[32] X. Liu, I. P. Udovichenko, S. D. M. Brown, K. P. Steel, and D. S. Williams, “Myosin

VIIa participates in opsin transport through the photoreceptor cilium," *J. Neurosci.*, vol. 19, no. 15, pp. 6267–6274, 1999, doi: 10.1523/jneurosci.19-15-06267.1999.

[33] I. Sahly *et al.*, "Localization of usher 1 proteins to the photoreceptor calyceal processes, which are absent from mice," *J. Cell Biol.*, vol. 199, no. 2, pp. 381–399, 2012, doi: 10.1083/jcb.201202012.

[34] A. Puppo *et al.*, "Retinal transduction profiles by high-capacity viral vectors," *Gene Ther.*, vol. 21, no. 10, pp. 855–865, 2015, doi: 10.1038/gt.2014.57.Retinal.

[35] E. Touchard *et al.*, "Suprachoroidal electrotransfer: A nonviral gene delivery method to transfect the choroid and the retina without detaching the retina," *Mol. Ther.*, vol. 20, no. 8, pp. 1559–1570, 2012, doi: 10.1038/mt.2011.304.

[36] X. Cai, Z. Nash, S. M. Conley, S. J. Fliesler, M. J. Cooper, and M. I. Naash, "A partial structural and functional rescue of a retinitis pigmentosa model with compacted DNA nanoparticles," *PLoS One*, vol. 4, no. 4, 2009, doi: 10.1371/journal.pone.0005290.

[37] S. Daya and K. I. Berns, "Gene therapy using adeno-associated virus vectors," *Clin. Microbiol. Rev.*, vol. 21, no. 4, pp. 583–593, 2008, doi: 10.1128/CMR.00008-08.

[38] L. H. Vandenberghe and A. Auricchio, "Novel adeno-associated viral vectors for retinal gene therapy," *Gene Ther.*, vol. 19, no. 2, pp. 162–168, Feb. 2012, doi: 10.1038/gt.2011.151.

[39] I. Bekerman, P. Gottlieb, and M. Vaiman, "Variations in Eyeball Diameters of the Healthy Adults," *J. Ophthalmol.*, vol. 2014, 2014, doi: 10.1155/2014/503645.

[40] R. R. Caspi, "A look at autoimmunity and inflammation in the eye," *J. Clin. Invest.*, vol. 120, no. 9, pp. 3073–3083, 2010, doi: 10.1172/JCI42440.

[41] R. Zhou and R. R. Caspi, "Ocular immune privilege," *Biol. Reports*, vol. 2, no. 1, pp. 1–3, 2010, doi: 10.3410/B2-3.

[42] S. Panda-Jonas, J. B. Jonas, M. Jakobczyk, and U. Schneider, "Retinal Photoreceptor Count, Retinal Surface Area, and Optic Disc Size in Normal Human Eyes," *Ophthalmology*, vol. 101, no. 3, pp. 519–523, 1994, doi: 10.1016/S0161-6420(94)31305-4.

[43] S. Remtulla and P. E. Hallett, "A schematic eye for the mouse, and comparisons with the rat," *Vision Res.*, vol. 25, no. 1, pp. 21–31, 1985, doi: 10.1016/0042-6989(85)90076-8.

[44] Q. Li *et al.*, "Intraocular route of AAV2 vector administration defines humoral immune response and therapeutic potential," *Mol. Vis.*, vol. 14, no. June, pp. 1760–

1769, 2008.

[45] N. Kumaran, M. Michaelides, A. J. Smith, R. R. Ali, and J. W. B. Bainbridge, “Retinal gene therapy,” *Br. Med. Bull.*, vol. 126, no. 1, pp. 13–25, 2018, doi: 10.1093/bmb/ldy005.

[46] K. Ding *et al.*, “AAV8-vectored suprachoroidal gene transfer produces widespread ocular transgene expression,” *J. Clin. Invest.*, vol. 129, no. 11, pp. 4901–4911, 2019, doi: 10.1172/JCI129085.

[47] G. Yiu *et al.*, “Suprachoroidal and Subretinal Injections of AAV Using Transscleral Microneedles for Retinal Gene Delivery in Nonhuman Primates,” *Mol. Ther. - Methods Clin. Dev.*, vol. 16, no. March, pp. 179–191, 2020, doi: 10.1016/j.omtm.2020.01.002.

[48] T. A. C. De Guimaraes, M. Georgiou, J. W. B. Bainbridge, and M. Michaelides, “Gene therapy for neovascular age-related macular degeneration: Rationale, clinical trials and future directions,” *Br. J. Ophthalmol.*, vol. 105, no. 2, pp. 151–157, 2021, doi: 10.1136/bjophthalmol-2020-316195.

[49] D. Dalkara and J. A. Sahel, “Gene therapy for inherited retinal degenerations,” *C. R. Biol.*, vol. 337, no. 3, pp. 185–192, 2014, doi: 10.1016/j.crvi.2014.01.002.

[50] K. I. Berns and C. Giraud, “Biology of adeno-associated virus.,” *Curr. Top. Microbiol. Immunol.*, vol. 218, pp. 1–23, 1996, Accessed: Mar. 03, 2017. [Online]. Available: http://www.ncbi.nlm.nih.gov/pubmed/8794242.

[51] F. Sonntag *et al.*, “The Assembly-Activating Protein Promotes Capsid Assembly of Different Adeno-Associated Virus Serotypes ▿ ,” *J. Virol.*, vol. 85, no. 23, pp. 12686–12697, 2011, doi: 10.1128/JVI.05359-11.

[52] B. S. and J. Chamberlain, “Recombinant Adeno-associated Virus Transduction and Integration,” *Mol. Ther.*, vol. 23, no. 1, pp. 1–7, 2008, doi: 10.1038/mt.2008.103.Recombinant.

[53] J. S. Bartlett, R. Wilcher, and R. J. Samulski, “Infectious entry pathway of adeno-associated virus and adeno-associated virus vectors.,” *J. Virol.*, vol. 74, no. 6, pp. 2777–85, Mar. 2000, Accessed: Mar. 04, 2017. [Online]. Available: http://www.ncbi.nlm.nih.gov/pubmed/10684294.

[54] D. Duan, Q. Li, A. W. Kao, Y. Yue, J. E. Pessin, and J. F. Engelhardt, “Dynamin is required for recombinant adeno-associated virus type 2 infection.,” *J. Virol.*, vol. 73, no. 12, pp. 10371–6, Dec. 1999, Accessed: Mar. 04, 2017. [Online]. Available: http://www.ncbi.nlm.nih.gov/pubmed/10559355.

[55] F. Sonntag, S. Bleker, B. Leuchs, R. Fischer, and J. A. Kleinschmidt, “Adeno-Associated Virus Type 2 Capsids with Externalized VP1/VP2 Trafficking Domains Are Generated prior to Passage through the Cytoplasm and Are Maintained until Uncoating Occurs in the Nucleus,” *J. Virol.*, vol. 80, no. 22, pp. 11040–11054, Nov. 2006, doi: 10.1128/JVI.01056-06.

[56] F. K. Ferrari, T. Samulski, T. Shenk, and R. J. Samulski, “Second-Strand Synthesis Is a Rate-Limiting Step for Efficient Transduction by Recombinant Adeno-Associated Virus Vectors,” *J. Virol.*, vol. 70, no. 5, pp. 3227–3234, 1996, Accessed: Mar. 04, 2017. [Online]. Available: https://www.ncbi.nlm.nih.gov/pmc/articles/PMC190186/pdf/703227.pdf.

[57] R. M. Kotin, R. M. Linden, and K. L. Berns, “Characterization of a preferred site on human chromosome 19q for integration of adeno-associated virus DNA by non-homologous recombination,” *EMBO J.*, vol. 1, no. 1, pp. 5071–5078, 1992, Accessed: Mar. 04, 2017. [Online]. Available: https://www.ncbi.nlm.nih.gov/pmc/articles/PMC556985/pdf/emboj00098-0395.pdf.

[58] D. Duan *et al.*, “Circular intermediates of recombinant adeno-associated virus have defined structural characteristics responsible for long-term episomal persistence in muscle tissue.,” *J. Virol.*, vol. 72, no. 11, pp. 8568–77, Nov. 1998, Accessed: Mar. 04, 2017. [Online]. Available: http://www.ncbi.nlm.nih.gov/pubmed/9765395.

[59] R. J. Samulski, K. I. Berns, M. Tan, and N. Muzyczka, “Cloning of adeno-associated virus into pBR322: rescue of intact virus from the recombinant plasmid in human cells.,” *Proc. Natl. Acad. Sci. U. S. A.*, vol. 79, no. 6, pp. 2077–81, Mar. 1982, Accessed: Mar. 04, 2017. [Online]. Available: http://www.ncbi.nlm.nih.gov/pubmed/6281795.

[60] L. H. Vandenberghe, J. M. Wilson, and G. Gao, “Tailoring the AAV vector capsid for gene therapy.,” *Gene Ther.*, vol. 16, no. 3, pp. 311–319, 2009, doi: 10.1038/gt.2008.170.

[61] D. H. Bryant *et al.*, “Deep diversification of an AAV capsid protein by machine learning,” *Nat. Biotechnol.*, 2021, doi: 10.1038/s41587-020-00793-4.

[62] R. Calcedo, L. H. Vandenberghe, G. Gao, J. Lin, and J. M. Wilson, “Worldwide epidemiology of neutralizing antibodies to adeno-associated viruses,” *J. Infect. Dis.*, vol. 199, no. 3, pp. 381–390, 2009, doi: 10.1086/595830.

[63] A. Asokan, D. V Schaffer, and R. Jude Samulski, “The AAV Vector Toolkit: Poised at

the Clinical Crossroads," *Mol. Ther.*, vol. 20, no. 4, pp. 699–708, Apr. 2012, doi: 10.1038/mt.2011.287.

[64] C. Lebherz, A. Maguire, W. Tang, J. Bennett, and J. M. Wilson, "Novel AAV serotypes for improved ocular gene transfer," *J. Gene Med.*, vol. 10, no. 4, pp. 375–382, 2008, doi: 10.1002/jgm.1126.

[65] M. Allocca *et al.*, "Novel Adeno-Associated Virus Serotypes Efficiently Transduce Murine Photoreceptors," *J. Virol.*, vol. 81, no. 20, pp. 11372–11380, 2007, doi: 10.1128/jvi.01327-07.

[66] A. J. Lotery *et al.*, "Adeno-Associated Virus Type 5: Transduction Efficiency and Cell-Type Specificity in the Primate Retina," *Hum. Gene Ther.*, vol. 14, no. 17, pp. 1663–1671, 2003, doi: 10.1089/104303403322542301.

[67] C. Mussolino *et al.*, "AAV-mediated photoreceptor transduction of the pig cone-enriched retina," *Gene Ther.*, vol. 18, no. 7, pp. 637–645, 2011, doi: 10.1038/gt.2011.3.

[68] K. Stieger *et al.*, "Subretinal delivery of recombinant AAV serotype 8 vector in dogs results in gene transfer to neurons in the brain," *Mol. Ther.*, vol. 16, no. 5, pp. 916–923, 2008, doi: 10.1038/mt.2008.41.

[69] L. H. Vandenberghe *et al.*, "Dosage Thresholds for AAV2 and AAV8 Photoreceptor Gene Therapy in Monkey," *Sci. Transl. Med.*, vol. 3, no. 88, 2011, doi: 10.1126/scitranslmed.3002103.Dosage.

[70] G. M. Acland *et al.*, "Long-Term Restoration of Rod and Cone Vision by Single Dose rAAV-Mediated Gene Transfer to the Retina in a Canine Model of Childhood Blindness," *Mol. Ther.*, vol. 12, no. 6, pp. 1072–1082, 2005, doi: 10.1016/j.ymthe.2005.08.008.Acland.

[71] G. M. Acland *et al.*, "Gene therapy restores vision in a canine model of childhood blindness," *Nat. Genet.*, vol. 28, no. 1, pp. 92–95, 2001, doi: 10.1038/ng0501-92.

[72] J. W. B. Bainbridge *et al.*, "Effect of Gene Therapy on Visual Function in Leber's Congenital Amaurosis," *N. Engl. J. Med.*, vol. 358, no. 21, pp. 2231–2239, 2008, doi: 10.1056/nejmoa0802268.

[73] W. W. Hauswirth *et al.*, "Treatment of Leber congenital amaurosis due to RPE65 mutations by ocular subretinal injection of adeno-associated virus gene vector: Short-term results of a phase I trial," *Hum. Gene Ther.*, vol. 19, no. 10, pp. 979–990, 2008, doi: 10.1089/hum.2008.107.

[74] P. D. Albert M. Maguire, M.D., Francesca Simonelli, M.D., Eric A. Pierce, M.D.,

Ph.D., Edward N. Pugh Jr., Ph.D., Federico Mingozzi, Ph.D., Jeannette Bennicelli, Ph.D., Sandro Banfi, M.D., Kathleen A. Marshall, C.O.T., Francesco Testa, M.D., Enrico M. Surace, D, "Safety and Efficacy of Gene Transfer for Leber's Congenital Amaurosis," *J. Med.*, vol. 358, no. 21, pp. 2240–2248, 2008, doi: 10.1056/NEJMoa0802315.Safety.

[75] M. C. Prof Jean Bennett, MD, Jennifer Wellman, MSc, Kathleen A Marshall, COT, Sarah McCague, BA, Manzar Ashtari, PhD, Julie DiStefano-Pappas, BA, Okan U Elci, PhD, Daniel C Chung, DO, Junwei Sun, MSc, J Fraser Wright, PhD, Dominique R Cross, MPH, Puya Aravand, "Safety and durability of effect of contralateral-eye administration of AAV2 gene therapy in patients with childhood-onset blindness caused by RPE65 mutatons: a follow-on phase 1 trial Prof," *Lancet*, vol. 388, no. 10045, pp. 661–672, 2017, doi: 10.1016/S0140-6736(16)30371-3.Safety.

[76] M. D. Fischer, "On Retinal Gene Therapy," *Ophthalmologica*, vol. 236, no. 1, pp. 1–7, 2016, doi: 10.1159/000445782.

[77] "FDA approves hereditary blindness gene therapy," *Nat. Biotechnol.*, vol. 36, no. 1, p. 7, 2018.

[78] I. Trapani and A. Auricchio, "Seeing the Light after 25 Years of Retinal Gene Therapy," *Trends Mol. Med.*, vol. 24, no. 8, pp. 669–681, 2018, doi: 10.1016/j.molmed.2018.06.006.

[79] B. L. Lam *et al.*, "Choroideremia Gene Therapy Phase 2 Clinical Trial: 24-Month Results," *Am. J. Ophthalmol.*, vol. 197, pp. 65–73, 2019, doi: 10.1016/j.ajo.2018.09.012.

[80] P. Yu-Wai-Man *et al.*, "Bilateral visual improvement with unilateral gene therapy injection for Leber hereditary optic neuropathy," *Sci. Transl. Med.*, vol. 12, no. 573, pp. 1–11, 2020, doi: 10.1126/scitranslmed.aaz7423.

[81] E. P. Rakoczy *et al.*, "Three-Year Follow-Up of Phase 1 and 2a rAAV.sFLT-1 Subretinal Gene Therapy Trials for Exudative Age-Related Macular Degeneration," *Am. J. Ophthalmol.*, vol. 204, pp. 113–123, 2019, doi: 10.1016/j.ajo.2019.03.006.

[82] C. Cukras *et al.*, "Retinal AAV8-RS1 Gene Therapy for X-Linked Retinoschisis: Initial Findings from a Phase I/IIa Trial by Intravitreal Delivery," *Mol. Ther.*, vol. 26, no. 9, pp. 2282–2294, 2018, doi: 10.1016/j.ymthe.2018.05.025.

[83] D. Duan, Y. Yue, and J. F. Engelhardt, "Expanding AAV Packaging Capacity with Trans-splicing or Overlapping Vectors: A Quantitative Comparison," *Mol. Ther.*, vol. 4, no. 4, pp. 383–391, Oct. 2001, doi: 10.1006/mthe.2001.0456.

[84] A. Ghosh, Y. Yue, Y. Lai, and D. Duan, “A Hybrid Vector System Expands Adeno-associated Viral Vector Packaging Capacity in a Transgene-independent Manner,” *Mol. Ther.*, vol. 16, no. 1, pp. 124–130, Jan. 2008, doi: 10.1038/sj.mt.6300322.

[85] Z. Yan, Y. Zhang, D. Duan, and J. F. Engelhardt, “Trans-splicing vectors expand the utility of adeno-associated virus for gene therapy.,” *Proc. Natl. Acad. Sci. U. S. A.*, vol. 97, no. 12, pp. 6716–21, Jun. 2000, doi: 10.1073/PNAS.97.12.6716.

[86] I. Trapani *et al.*, “Effective delivery of large genes to the retina by dual AAV vectors,” *EMBO Mol. Med.*, vol. 6, no. 2, pp. 194–211, 2014, doi: 10.1002/emmm.201302948.

[87] Y. Lai *et al.*, “Efficient in vivo gene expression by trans-splicing adeno-associated viral vectors,” *Nat. Biotechnol.*, vol. 23, no. 11, pp. 1435–1439, Nov. 2005, doi: 10.1038/nbt1153.

[88] S. J. Reich *et al.*, “Efficient Trans-Splicing in the Retina Expands the Utility of Adeno-Associated Virus as a Vector for Gene Therapy,” *Hum. Gene Ther.*, vol. 14, no. 1, pp. 37–44, Jan. 2003, doi: 10.1089/10430340360464697.

[89] A. Ghosh, Y. Yue, and D. Duan, “Viral serotype and the transgene sequence influence overlapping adeno-associated viral (AAV) vector-mediated gene transfer in skeletal muscle.,” *J. Gene Med.*, vol. 8, no. 3, pp. 298–305, Mar. 2006, doi: 10.1002/jgm.835.

[90] P. Colella *et al.*, “Myosin7a Deficiency Results in Reduced Retinal Activity Which Is Improved by Gene Therapy,” *PLoS One*, vol. 8, no. 8, 2013, doi: 10.1371/journal.pone.0072027.

[91] P. Colella *et al.*, “Efficient gene delivery to the cone-enriched pig retina by dual AAV vectors,” *Gene Ther.*, vol. 21, no. 4, pp. 450–456, 2014, doi: 10.1038/gt.2014.8.

[92] A. L. M. Bothwell, M. Paskind, M. Reth, T. Imanishi-Kari, K. Rajewsky, and D. Baltimore, “Heavy chain variable region contribution to the NPb family of antibodies: somatic mutation evident in a γ2a variable region,” *Cell*, vol. 24, no. 3, pp. 625–637, 1981, doi: 10.1016/0092-8674(81)90089-1.

[93] A. M. D. Amit C Nathwani , John T Gray, Catherine Y C Ng, Junfang Zhou, Yunyu Spence, Simon N Waddington, Edward G D Tuddenham, Geoffrey Kemball-Cook, Jenny McIntosh, Mariette Boon-Spijker, Koen Mertens, “Self-complementary adeno-associated virus vectors containing a novel liver-specific human factor IX expression cassette enable highly efficient transduction of murine and nonhuman primate liver,” *Blood*, vol. 107, no. 7, pp. 2653–2661, 2006, doi: 10.1182/blood-

2005-10-4035.Supported.

[94] K. R. and J. K. D. Grimm, A. Kern, “Novel Tool for Production and Purification Recombinant Adenoassociated Virus Vectors,” *Hum. Gene Ther.*, vol. 2760, pp. 2745–2760, 1998.

[95] Y. L. Liu *et al.*, “Optimized production of high-titer recombinant adeno-associated virus in roller bottles,” *Biotechniques*, vol. 34, no. 1, pp. 184–189, 2003, doi: 10.2144/03341dd07.

[96] A. Salvetti *et al.*, “Factors influencing recombinant adeno-associated virus production,” *Hum. Gene Ther.*, vol. 9, no. 5, pp. 695–706, 1998, doi: 10.1089/hum.1998.9.5-695.

[97] S. Zolotukhin *et al.*, “Recombinant adeno-associated virus purification using novel methods improves infectious titer and yield,” *Gene Ther.*, vol. 6, no. 6, pp. 973–985, 1999, doi: 10.1038/sj.gt.3300938.

[98] M. Doria, A. Ferrara, and A. Auricchio, “AAV2/8 vectors purified from culture medium with a simple and rapid protocol transduce murine liver, muscle, and retina efficiently,” *Hum. Gene Ther. Methods*, vol. 24, no. 6, pp. 392–398, 2013, doi: 10.1089/hgtb.2013.155.

[99] F. Gibson *et al.*, “A type VII myosin encoded by the mouse deafness gene shaker-1,” *Nature*, vol. 374, no. 6517. pp. 62–64, 1995, doi: 10.1038/374062a0.

[100] F.-Q. Liang, V. Anand, A. M. Maguire, and J. Bennett, “Intraocular Delivery of Recombinant Virus,” *Vis. Res. Protoc.*, vol. 47, pp. 125–139, 2000, doi: 10.1385/1-59259-085-3:125.

[101] H. R. Kim, H. W. Rho, J. W. Park, B. H. Park, J. S. Kim, and M. W. Lee, “Assay of Ornithine Aminotransferase with Ninhydrin,” *Analytical Biochemistry*, vol. 223, no. 2. pp. 205–207, 1994, doi: 10.1006/abio.1994.1574.

[102] J. I. Juncosa, H. Lee, and R. B. Silverman, “Two continuous coupled assays for ornithine-δ-aminotransferase,” *Anal. Biochem.*, vol. 440, no. 2, pp. 145–149, 2013, doi: 10.1016/j.ab.2013.05.025.

[103] J. F. Wright *et al.*, “Identification of factors that contribute to recombinant AAV2 particle aggregation and methods to prevent its occurrence during vector purification and formulation,” *Mol. Ther.*, vol. 12, no. 1, pp. 171–178, 2005, doi: 10.1016/j.ymthe.2005.02.021.

[104] A. Maddalena *et al.*, “Triple Vectors Expand AAV Transfer Capacity in the Retina,” *Mol. Ther.*, vol. 26, no. 2, pp. 524–541, 2018, doi: 10.1016/j.ymthe.2017.11.019.

[105] T. Wang, G. Steel, A. H. Milam, and D. Valle, “Correction of ornithine accumulation prevents retinal degeneration in a mouse model of gyrate atrophy of the choroid and retina,” *Proc. Natl. Acad. Sci. U. S. A.*, vol. 97, no. 3, pp. 1224–1229, 2000, doi: 10.1073/pnas.97.3.1224.

[106] R. E. MacLaren *et al.*, “Retinal gene therapy in patients with choroideremia: initial findings from a phase 1/2 clinical trial,” *Lancet*, vol. 383, no. 9923, pp. 1129–1137, Mar. 2014, doi: 10.1016/S0140-6736(13)62117-0.

[107] M. I. Patrício, C. I. Cox, C. Blue, A. R. Barnard, C. Martinez-Fernandez de la Camara, and R. E. MacLaren, “Inclusion of PF68 Surfactant Improves Stability of rAAV Titer when Passed through a Surgical Device Used in Retinal Gene Therapy,” *Mol. Ther. - Methods Clin. Dev.*, vol. 17, no. June, pp. 99–106, 2020, doi: 10.1016/j.omtm.2019.11.005.